

POLITECNICO DI TORINO

Department of Mechanical and Aerospace Engineering (DIMEAS)
Master's degree in biomedical engineering



**Reproducing cardiac fibrosis: from state of the art analysis to the design
of bioartificial electrospun fibers for *in vitro* pathological cardiac tissue
modelling**

Candidate
Fabio Carangelo

Supervisor
Proff.ssa Valeria Chiono

Co-supervisor
Dott.ssa Irene Carmagnola

Academic Year 2019/2020

Index

Abstract	4
1) Introduction	6
1.1) Aim of the work.....	6
1.2) Heart physiology.....	7
1.2.1) Cardiac fibroblast.....	7
1.2.2) Bioactivity and homeostasis of extracellular matrix.....	8
1.2.3) Differentiation into myofibroblast.....	8
1.2.4) Development of fibrosis.....	10
1.2.5) Myocardial infarction.....	10
1.3) Treatment overview.....	11
4) Tissue engineering.....	12
1.5) Role of <i>in vitro</i> models as platform for drug testing.....	14
6) Material used in <i>in vitro</i> cardiac models.....	15
1.6.1) Synthetic fibrous cardiac models.....	15
1.7) 2D models.....	17
1.7.1) Cell micropatterning for 2D CM alignment.....	19
1.8) 3D cardiac tissue models.....	20
1.8.1) 3D matrices production.....	21
2) State of art for <i>in vitro</i> cardiac model	25
2.1) Electrospinning models.....	25
2.2) Coating strategies for cardiac cells culture.....	27
2.3) Coating with a layer of Polydopamine.....	28
2.4) Plasma grafting and plasma treatment.....	31
2.5) Model validation strategies.....	35
2.6) Methods to distinguish cardiac fibroblasts from myofibroblasts.....	43
3) Materials and methods	51
3.1) Polycaprolactone.....	51
3.2) Electrospinning.....	51
3.2.1) Process optimization.....	52
3.2.2) Membranes fabrication.....	53
3.4) Functionalization process.....	54
3.4.1) Polydopa-gelatin functionalization.....	54
3.5) PCL Scaffolds characterizations.....	55
3.5.1) Scanning Electron Microscope (SEM).....	55
3.5.2) ImageJ Software.....	55

3.5.3) Contact angle	55
3.5.4) Solvent casting.....	56
3.5.5) Acid Orange UV-Vis	57
3.5.6) Degradation Analysis.....	58
4) Results	59
4.1) Scaffold fabrication.....	59
4.1.1) Scanning Electron Microscopy (SEM)	59
4.1.2) ImageJ software	61
4.1.3) Degradation Analysis.....	63
4.2) Scaffold functionalization.....	64
4.2.1) Contact angle	64
4.2.1) Acid Orange UV-Vis	65
5) Conclusions.....	68
Bibliography	70
Ringraziamenti	74

Abstract

Heart disease is the leading cause of mortality worldwide. After a stroke a lot of cardiac cells are lost, especially cardiomyocytes. Then a reparative wound process starts, including the proliferation and activation of cardiac fibroblasts into myofibroblasts, the production of new extracellular matrix (ECM) and the increasing of type I and III collagen content. All these events lead to myocardial fibrosis and cardiac tissue stiffening. Heart pump capacity results to be impaired and heart failure can occur. Since cardiomyocytes are not able to replicate, scar tissue will not become functional anymore, so heart function will no longer be restored. Nowadays there are no therapies promoting heart regeneration and heart transplantation remains the only available clinic approach. However, this option shows some restrictions related to the lack of donors and the risk of rejection.

To overcome the limitations associated with transplantation, new strategies for infarcted myocardial regeneration are under investigation. In this contest, *in vitro* models of human cardiac tissue are useful tool for preclinical screening, overcoming the low predictability of *in vivo* animal tests.

In this thesis work, an analysis about the state of art of *in vitro* cardiac disease modelling was conducted. This work focused on the study of tissue engineered constructs aiming to produce *in vitro* models of myocardial fibrosis. Besides, we investigated the main approaches used to distinguish myofibroblast phenotype from cardiac fibroblast one by detecting specific markers such as Alpha smooth muscle actin (α -SMA), Angiotensin 1 receptor (AT1) and fibronectin extra dominant A.

In the experimental section, electrospinning was used to fabricate a biomimetic scaffold for human cardiac fibroblasts culture.

The work focused on the optimization of a previous set of parameters for the electrospinning of PCL (Mw=43 kDa) random fibers. A step forward was done by testing a new set of parameters to produce aligned nanofibrous scaffolds. PCL random scaffolds mimic the morphology of early-stage myocardial fibrotic ECM while the aligned PCL scaffolds reproduce the end-stage of fibrosis in which the contraction and the stress make the orientation anisotropic.

Gelatin (G) was grafted on electrospun scaffolds to improve their wettability and biomimicity. Gelatin coming from collagen denaturation and as demonstrated in literature is a good substrate for human cardiac fibroblasts cultures. G was deposited on the scaffolds

through a mussel-inspired approach, by using 3,4-Dihydroxy-DL-phenylalanine (DOPA) as an adhesive pre-coating. Physic-chemical and morphological analysis were carried out to assess the quality of scaffold and functionalization process. Degradation analysis showed PCL scaffolds degrade only in a few percentages, remaining stable during the range of time considered (4.25% at 28 days). Contact angle at 5s displayed the correct functionalization with G, since the contact angle had the major decrease with the polyDOPA/G bi-layer (62°). Acid Orange UV-Vis colorimetric assay also confirmed the efficiency of functionalization protocol. The number of moles per cm^2 was assessed by this analysis in three-time steps (1gg, 3gg and 7gg) to characterize the stability of the coating during this period. PolyDOPA/Gelatin scaffold gave the best results in all the three-time steps (0.0043 n mol/ cm^2 at 1 day, 0.0033 n mol/ cm^2 at 3 days and 0.0046 n mol/ cm^2 at 7 days).

1) Introduction

1.1) Aim of the work

The development of a new drug requests *in vivo* trials that involve first animals and then humans, bringing to some ethical, safety and economic issues.

In vitro models try to overcome the limitations associated with animal experimentation in agreement with 3R principle . The use of *in vitro* human models, faithfully mimicking native tissues architecture, conducts to more reliable results about the chemotoxicity during preclinical drug screening.

The aim of this thesis work was to research previous works on *in vitro* fibrotic cardiac models and then choose the best strategies to fabricate a biomimetic scaffold for human cardiac fibroblasts culture. Then a summary was made by tacking the highlights of the works found. Coating was used to improve the biocompatibility and biomimecity of the scaffold. This aim is reached by using proteins such as collagen, gelatin or fibronectin to cover the scaffold surface. However, a simple dive in the protein is not enough, because the grafting would be not very stable. That is why covalent coating must be used with technique such as plasma treatment or polydopamine coating.

In the experimental section, electrospun PCL scaffolds were fabricated by using the electrospinning technique.

A gelatin layer was made to decrease the contact angle of the material, since PCL nanofibers had a low wettability and cells scarcely linked on it. A previous layer of polydopamine was realized to make the Gelatin deposition more efficient.

These biomimetic electrospun scaffolds can be used for the seeding of human cardiac fibroblasts and can be proposed as substrates for s *in vitro* fibrotic heart model on which a direct cell reprogramming therapy can be tested.

Some strategies can be used to validate the model and to evaluate fibroblasts activation, Immunochemistry and PCR are techniques that allow the validation of the model since detect the markers expressed from cells.

These strategies can be used to assess the presence of myofibroblasts by detecting the presence of specific markers such as Alpha smooth muscle actin (α -SMA), Angeotensin 1 (AT 1), transforming growth factor- β type II receptor, paxillin, tensin, and fibronectin extra dominant A, since some of them are higher expressed in myofibroblasts respect to cardiac fibroblasts and others are expressed only in myofibroblasts.

Then it was found that at the beginning of the fibrosis some genetic markers were downregulated in myofibroblasts such as miR-29. The presence of these RNA fragments was assessed by using PCR. So, this technique can be used in combination with markers above mentioned to validate the presence of this kind of cells.

1.2) Heart physiology

The heart is a dynamic architecture of connective tissue and several cardiac cell types that add different qualities to the myocardium. However, cardiomyocytes are the fundamental source of cardiac contractility, the non-myocyte fraction, including endothelial cells, macrophages, smooth muscle cells, and fibroblasts, are also important cellular constituents of both the healthy and the sick heart [1].

Cardiac fibroblasts have an important structural and functional role that ensure structural support, uniform contractility, and homeostasis of the extracellular matrix.

ECM homeostasis is preserved by production and secretion of connective tissue proteins, such as elastin and collagens. The opposite mechanism is degradation of proteins by specific proteases. Some events can alter the homeostasis, such as aging, exposure to certain drugs, or in response to various heart disease, such as myocardial infarction and hypertension [2]. This disequilibrium leads the heart to undergoes spatial and temporal remodeling events that can bring to fibrosis, a pathological state characterized by the excessive accumulation of fibrous connective tissue.

1.2.1) Cardiac fibroblast

Cardiac fibroblast accounting for 60%-70% of the cell population of the myocardium, approximately 20% by volume. Cardiac fibroblasts have a structure similar to that of fibroblast of other organs of the body for what concern structural and ECM-regulating function, but they have a different response to stimuli, suggesting high organ specificity [3,4].

Fibroblasts are mesenchymal cells, they are spindle-shaped granular cells bereaved of a basement membrane. They are the principal producer of ECM in the heart, which provides support for cardiomyocytes, ensuring the functional integration of mechanical forces in the beating heart. While other major cells of the myocardium, such as pericytes, endothelial cells, and smooth muscle cells, are confined to the vasculature.

They are tightly integrated in the endomysial collagen network and organized in lamella around groups of cardiomyocytes [5,6]. This leads to a strongly response to mechanical, electrical, and chemical stimuli.

Direct interactions between CFs and ECM are mediated by integrins and discoidin domain receptor-2 (DDR2), a collagen receptor. Further cellular interfaces and contacts are ensured by cadherins (N-cadherin, cadherin 11) and connexins. CFs form intercellular gap junctions through connexin40, while connexin45 is involved in gap junctions with cardiomyocytes, furthermore they are associated with ability to synthesize a plethora of bioactive molecules [7].

1.2.2) Bioactivity and homeostasis of extracellular matrix

The daily ECM turnover rate is estimated to be 5% under physiologic conditions. From this parameter we can differentiate a normal cardiac development, pathological responses, and optimal heart function.

CFs produce most of structural and bioactive components that constitute the highly differentiate ECM under physiological conditions. Important properties of the ECM, such as tensile strength and elasticity, come from collagen fibrils and elastin. CFs are also important since they produce adhesive proteins linked to cell signaling. Both structural and functional properties are also improved by CF-derived proteoglycans secreted into interstitial space.

Thanks to proteolytic enzymes produced by CFs the degradation of ECM is promoted, the most abundant of these enzymes are zinc-dependent matrix metalloproteinases (MMPs).

To avoid uncontrolled matrix degradation CFs produce endogenous MMPs inhibitors, defined tissue inhibitors of metalloproteinases that bind to active sites of MMPs.

ECM is produced and remodeled not only from CFs, but also from cardiomyocytes, endothelial cells, and smooth muscle cells that are sources of collagen and fibronectin [8].

1.2.3) Differentiation into myofibroblast

Myofibroblasts (myoFbs) refers to activated and fibrosis-mediating CFs, arising by differentiation of CFs upon chemical or mechanical stimuli. Compared to CFs, myoFbs have a higher activity of ECM production, which manifests in net deposition of matrix proteins, especially collagens and fibronectin (**Fig 1a**). MyoFbs produce a plethora of bioactive

molecules, including growth factors, cytokines, and proteases. They also produce a special group of matricellular proteins [5, 6, 7, 8].

Besides, upregulation of a large number of smooth muscle genes is linked with myoFb differentiation, including tropomyocin, transgelin, SMemb/nonmuscle myosin heavy chain-B, and α -smooth muscle actin (α -SMA). The molecule is associated with characteristic stress fiber formation (**Fig 1b**).

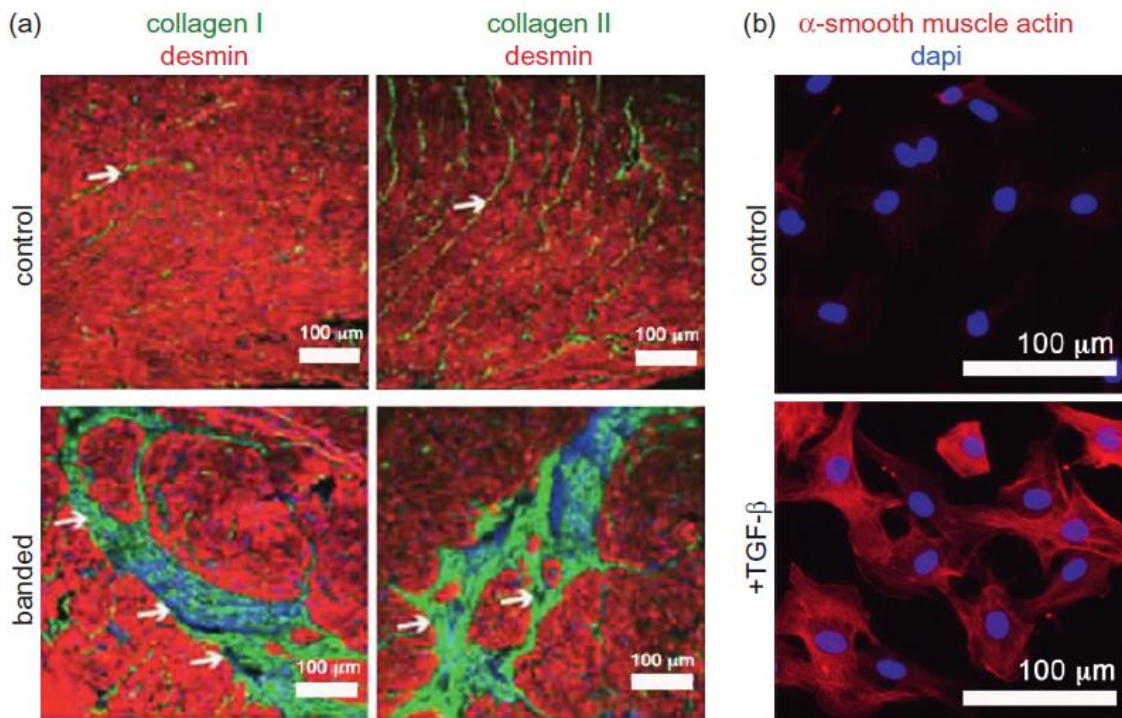


Fig 1. Myofibroblast (myoFbs) are drivers of cardiac fibrosis. (a) The white arrows indicate a deposition of matrix in the interstitial space that characterize the cardiac fibrosis, this is an accumulation of collagen I and III in a pressure-overload mouse heart. Desmin marks cardiomyocytes, pericytes, and smooth muscle cells. (b) Five days in vitro culture of primary rat cardiac fibroblasts (CFs) induced by 48 hours of TGF- β incubation tp myoFbs, as displayed by stress fiber formation of α -smooth muscle actin. Nuclei was stained with Dapi [6].

Myofibroblasts are activated CFs that come from differentiation of CFs through mechanical and chemical stimuli due to the fibrosis. Myofibroblast have an augmented ECM production, with the consequence of a net deposition of matrix proteins, principally collagen and fibronectin.

Myofibroblast can be distinguished from CFs by Golgi apparatus and rough endoplasmic reticulum. Smooth muscle cells and pericytes can be distinguished from myoFbs thanks to their desmin expression and heavy chain of smooth muscular myosin.

There is an intermediate status of the differentiation, protomyofibroblasts, which is accomplished by transforming growth factor (TGF). In fact, it can lead to a full differentiation in myofibroblast displaying α -SMA stress fibers, high production of matrix, and supermature focal adhesion.

The progression of pathological cardiac fibrosis might occur due to the lack of de-differentiation or apoptotic signals in myoFbs, as they persist in the injured heart [9, 10].

1.2.4) Development of fibrosis

Cardiac fibrosis is an end-point adaptation process of the cardiac remodeling process in the myocardium. A mechanical, chemical, or electric stress from ECM, immune cells, or cardiomyocytes can act as input to initiate this events cascades. As soon as change happens in CFs, injured signals augment by molecule secretions auto and paracrine. Hence CFs are good signals indicate a remodeling in progress. Even if the process of remodeling is an adaptive response to molecular injured signals, biased pro-fibrotic signals and lack of attenuation activity of myoFbs can lead to a maladjustment. This leads to substantial difference between initial damage and stress signals. Notwithstanding, fibrosis develop a “replacement fibrosis” or a “reactive fibrosis”, depending on whether the process is repair driven or by death myocytes or whether the process is driven by secondary, non-injured sites [11,12,13].

1.2.5) Myocardial infarction

Myocardial infarction is followed by a repair-driven response, which occurs to replace cardiomyocyte loss with a scar of connective tissue. A fibrin-based matrix is created serving to support the invading inflammatory cells and CFs [14].

At the beginning, the apoptotic and primarily necrotic cardiomyocytes provide the signals that attract immune cells and CFs to the infarct zone. While the inflammatory phase generally starts between 1 hour to 4 days after the infarct, matrix degradation by MMPs can already be detectable after 15-30 minutes [15]. Matrix degradation can increase inflammation by producing matrix fragments, such as matrikines along with proteolytic activation of tumor necrosis factor-alpha (TNF- α). On the other hand, MMPs can also negatively modulate chemokine activities through truncation and proteolysis [16,17].

The temporary upregulation of frizzled-2 protein attracts CFs/myoFbs to the infarct area. MyoFb differentiation is mediated by hypoxia and pro-fibrotic effectors such as AngII and TGF- β , and it is recognizable from both increasing in collagen synthesis and releasing of pro-inflammatory TNF- α and pro-angiogenic VEGF [18]. Furthermore, in infarcted area, reperfusion return will promote myoFb differentiation. The myoFbs facilitate a sustained wound contraction, which is controlled by humoral factors, such as AngII. MyoFbs can persist in a healed infarcted heart for up to 20 years, to ensure ECM maintenance and protection from repetitive stress due to the heart beating [19].

In cardiac fibrosis related to infarction, the initial adaptive replacement fibrosis of the infarct may eventually turn maladaptive, and collagen I deposition with increased cross-linking is observed in areas distant from the initial insult. This reactive fibrosis can contribute to development of heart failure, along with detrimental events related to the injury site, such as wall thinning and increase of infarct area.

Cardiac rupture is a fatal consequence of myocardial infarction and arises from excessive matrix degradation in the early phases of remodeling, possibly combined with a delayed or impaired production of connective tissue in later phases of remodeling, possibly combined with a delayed or impaired production of connective tissue in later phases [20].

1.3) Treatment overview

Heart attack symptoms can vary as the left arm pain, chest pain, nausea, difficulty breathing, dizziness and fainting. Injury blood analysis are performed to find specific markers to diagnose a heart attack. Another test is electromyography that is performed to search for significant variations in the electric heart activity.

Once the heart attack has been diagnosed the therapies can be the following:

1. Pharmacologic therapy; it includes those drugs that keep the blood fluid such as aspirin, anticoagulants, vasodilators, and antiplatelet agents. Another kind of drugs are thrombolytics, that must be taken in 12 hours otherwise their risks overcome the benefits.
2. Coronary artery bypass graft; through this technique a bridge is created to overcome what is blocking the blood. Besides, can be used angioplasty instead of the coronary artery bypass graft. In this way the blood stream is restored by cleaning the vessel through inflation and deflation of a balloon inserted in the occluded vessel .
3. Heart transplant; this is the more complex and expensive solution due to compatible donor lack and moreover transplantation list is very long.

4. Cellular therapy; this is an experimental technique that consists in injecting cardiac or stem cells that will become myocytes directly in the site of the injury restoring the damaged tissues. However, it is not so effective because most cells die without adhere to the tissue.

5. Scaffold implant; this is another experimental technique. Like cellular therapy, it is to try to repair the injured by placing cardiac or stem cells. In this case the cells are inserted in a scaffold that gave protection, signals and support to them. The major problem of the cellular therapy is that the environment of the damaged area is very aggressive, due to the inflammation generated from the stroke. This leads to an acidic pH and to an increased presence of immune cells. The cells go against apoptosis because them do not receive the correct signals to grow up and differentiate correctly. Instead by placing them on a scaffold that acts like a substrate and it can give them the correct signals for a certain time, the cells can integrate with the environment rightly. When the cells have achieved the correct differentiation and they are properly incorporated the scaffold must degrade.

1.4) Tissue engineering

Tissue engineering is a discipline that deals with regeneration of a damaged component of the human body or with the creation of constructs with similar characteristic to those of the tissues to make some study with them. The regenerative component gets ideas from some animals that can regenerate their organs much higher than that of the human beings. To do so tissue engineering requires some fundamentals (**Fig 2**). Of these fundamentals the most critical is cells. The principal kind of cells exploited are staminal cells. There are various types of staminal cells, and everyone have its power, that is the capability to differentiate in a certain type of cell. There are pluripotent staminal cells with the characteristic to differentiate in various types of cells. Embryonic stem cells belong to this category. In the last few years genetic therapy has been started to use on cells already differentiated, creating induced stem cells (iPS). Those cells are at the base of in vitro tissue model used for testing drugs and to avoid ethical problems for animal experimentation.

However, we have to considerate the complexity of such a model. In fact, organs make up the human body are composed by various type of cells, so to form the model we should take in account the different factors that the cells need. That is why the approach of tissue engineering point to replace prosthesis, artificial organs or transplant with regeneration of the native tissue itself, in order to avoid rejections due to incompatibility and prosthesis

ruptures. The principal components of the regenerative medicine are human cells, that can be:

- Specialized somatic
- Adult staminal
- Derived from embryonic staminal cells
- “reprogrammed” somatic cells and induced to pluripotency

The last have a lot of importance for the fact that the first have less availability of the most specialized somatic cells, adult staminal cells are difficult to expand and the derived from embryonic stem cells have ethic problems. Engineering technics exploit mainly scaffolds as tridimensional and bidimensional template to stick, proliferate and differentiate cells both *in vitro* and *in vivo*. The implant must have a porous structure to have optimal results and it must have interconnected porosity, mechanical propriety like those of the target tissue, it must be biodegradable, bioresorbable and biocompatibility, as well as its degradation products.

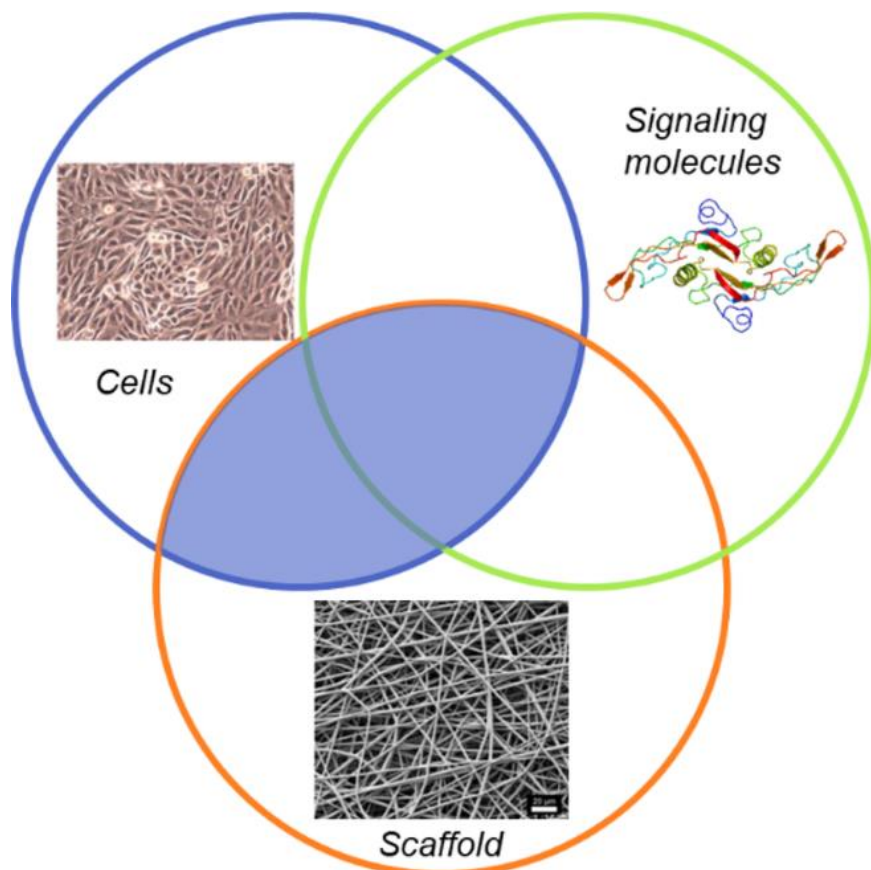


Fig 2. Basic tissue engineering requirements.

1.5) Role of *in vitro* models as platform for drug testing

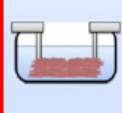
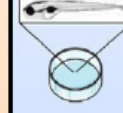
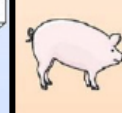
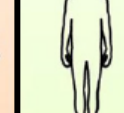
Drug development requires a great effort in terms of time and economic resource. The development cost raises especially in the latest stage when the experiments on animal and human start. The worst case scenario for a pharmaceutical company is to fail during this latest tests. Because of this reason many pharmaceutical companies follow a “fail early, fail cheap” approach. Cardiac side effects such as arrhythmias are the most common reason for the withdrawal of drugs. An estimated ~ 45% of all withdrawals and ~ 30% of restrictions to drug application are due to unwanted cardiovascular effects. This have brought US and UE agencies to establish guidance for industry. Though the currently approved test systems increased the sensitivity for the detection of certain side effects, they still have major shortcomings, including the lack of consideration of species difference and complex interactions between more than one ion channel.

The use of Human induced pluripotent stem cell-derived cardiomyocytes (HiPSC-CM) can be a possible solution to overcomes the problem in the use of a human heart as test-bed for the prediction of side effects . HiPSC-CM has a lot of similarities with structural and regulatory elements present in a human CM. HiPSC-CMs are smaller, beat spontaneously, show a lower degree of ultrastructural organization, have no t-tubules, less negative diastolic membrane potential, slower action potential upstroke velocity and lower contractile force, and smaller responses to beta-adrenergic stimulation or the Ca^{2+} -channel agonist Baay K 8644.

Another advantage on the use of *in vitro* models is the reduction in the economic and ethical cost of animal models. Moreover, the animal physiology is different from humans, so it cannot be so predictive.

An experimentation required different animals of different scales, so if a company employ an *in vitro* model rather than animals it will decrease the expense for the research. It also avoids the step for the human experimentation and its relative cost [21].

An overview of the current methods is presented in **Fig 3**.

	Expression systems	Isolated cardio-myocytes, 2D	Engineered heart tissue	Langendorff setup	Zebrafish	Large animal models	Clinical studies
Material/ Method							
Output	I_{Kr} inhibition (direct/indirect)	Ion currents, APs, Triggered activity	Contraction, APs, Triggered activity	Repolarization, Contraction, Reentry, Triggered activity	Repolarization, Contraction, Triggered activity	Repolarization, Contraction, Arrhythmias	Repolarization, Arrhythmias, (from ECG/holder)
Species	Heterologous	Various animals, Humans (limited, atria only, ESC/iPSC-derived cells)	Various animals, Humans (iPSC-derived cells)	Various animals, Humans (rare)	Zebrafish	Dog, Goat, Pig, Sheep	Humans
Main Properties	High throughput, Single cell, Single ion current, Acute effects only	Relatively low (primary culture) to high throughput (ESC/iPSC-derived cells), Effects on multiple ion currents, Acute effects only, Disease-specific models	Medium throughput, Multi-cellular, Effects on multiple ion currents, Acute and long-term effects, Disease-specific models	Relatively low (primary culture) to high throughput (ESC/iPSC-derived cells), Effects on multiple ion currents, Acute effects only, Disease-specific models	Medium throughput, Multi-cellular, Effects on multiple ion currents, Acute and long-term effects, Disease-specific models	Low throughput, In vivo, Multiple ion currents, Acute and long-term effects, Pathophysiological conditions, All types of arrhythmias	Low throughput, In vivo, Multiple ion currents, Acute and long-term effects, Different clinical settings, All types of arrhythmias

← Translational gap →

← Increasing levels of integration →

Fig 3. Characteristics of current technique in cardiac pharmacology with complexity increasing from left to the right. Approved procedures are in green. Methods occasionally used are in orange. New projects are in blue. Engineered heart tissue (red border) generated from hiPSC-CM might bridge the gap between complexity, cost-effective and a high predictive value [21].

1.6) Material used in *in vitro* cardiac models

Biomaterials play a fundamental role in creating 3D tissue model, since they are not only a support for cell attachment, but they also transmit load, provide a stiffness similar to that of physiological tissue, and they can be degraded by the proteins secreted by the cells.

1.6.1) Synthetic fibrous cardiac models

Synthetic biomaterials can be good for researchers as process, mechanical properties, topography, and structure of the material can be well controlled. Various synthetic polymers

were used to build up 3D cardiac scaffolds for the *in vitro* and *in vivo* models. The materials must emulate the original tissue in 3D hierarchical structure, demonstrate mechanical integrity and possess the correct surface properties. The most frequently used synthetic polymers for cardiac tissue engineering are polyurethane, poly ϵ -caprolactone (PCL), polylactic acid (PLA), polyglycolic acid (PGA), and their copolymers. One example of synthetic material-based cardiac constructs were generated with neonatal rat CMs and poly(glycerol sebacate) (PGS) and maintained in a bioreactor with simultaneous culture medium perfusion and electrical conditioning, which led to enhanced organization and functionality of engineered cardiac tissue.

Electrospinning is a technique to obtain cell alignment in a nanofiber-based scaffold, which provide guidance and support for the CMs. CMs tend to follow the nanostructure of the scaffold and organize themselves in an anisotropic structure to mimic the structure of ECM in myocardium.

The properties of the myocardial tissue are defined also by orientation and density of electrospun polymethylglutamide (PMGI) nanofibers. These two parameters are optimized for best alignment with 30-50 fibers/mm and an average distance between fibers of under 30 μm . An aligned fibrous mesh of electrospun polyester blend, poly(3-hydroxybutyrate-co-3-hydroxyvalerate) (PHBV), P(L-D,L)LA, and poly(glycerol sebacate) (PGS) was shown to enhance cardiomyogenic differentiation of human umbilical cords mesenchymal stem cells. Similarly, to promote sarcomere formation in CMs we can use rotary jet spinning to fabricate highly aligned nanofiber constructs from a blend of collagen, gelatin, and PCL polymer.

Even if the electrospun 3D scaffolds was made with aligned synthetic polymers nanofibers and they have similar characteristic to the native myocardial ECM, the lack of enough space between the porosity impede cell infiltration into the matrix and therefore the real structure is limited to a 2D space. To overcome this problem, a highly defined scaffold structure was fabricated by two-photon initiated polymerization (TPIP) and this have given the possibility to control a lot of matrix features.

The various search suggest that 3D tissue engineered models with controlled cellular microenvironments is a great hope for drug screening and cardiotoxicity testing. By putting together biomaterials with existing iPSC-based disease models could better be representative of disease pathology and they can display a better scalability for arriving to personalized models to meet different and urgent patient needs [22].

1.7) 2D models

PCL is an FDA approved, biodegradable and biocompatible polymer, widely used for *in vivo* and *in vitro* applications. However, unmodified PCL is characterized by a low hydrophilicity that drastically reduces cell affinity.

Shin *et al.* [21] demonstrated electrospun PCL membranes on wire rings could stand the load of a beating heart .

Blending PCL with some biomolecules could provide scaffolds with better biocompatibility, hydrophilicity, and more suitable mechanical properties for cardiac TE. In this study, a PCL/Gelatin blend (PG) was electrospun in order to obtain both random and aligned nanofibers.

Hydrophilicity increased as it is shown by graph (fig 4).

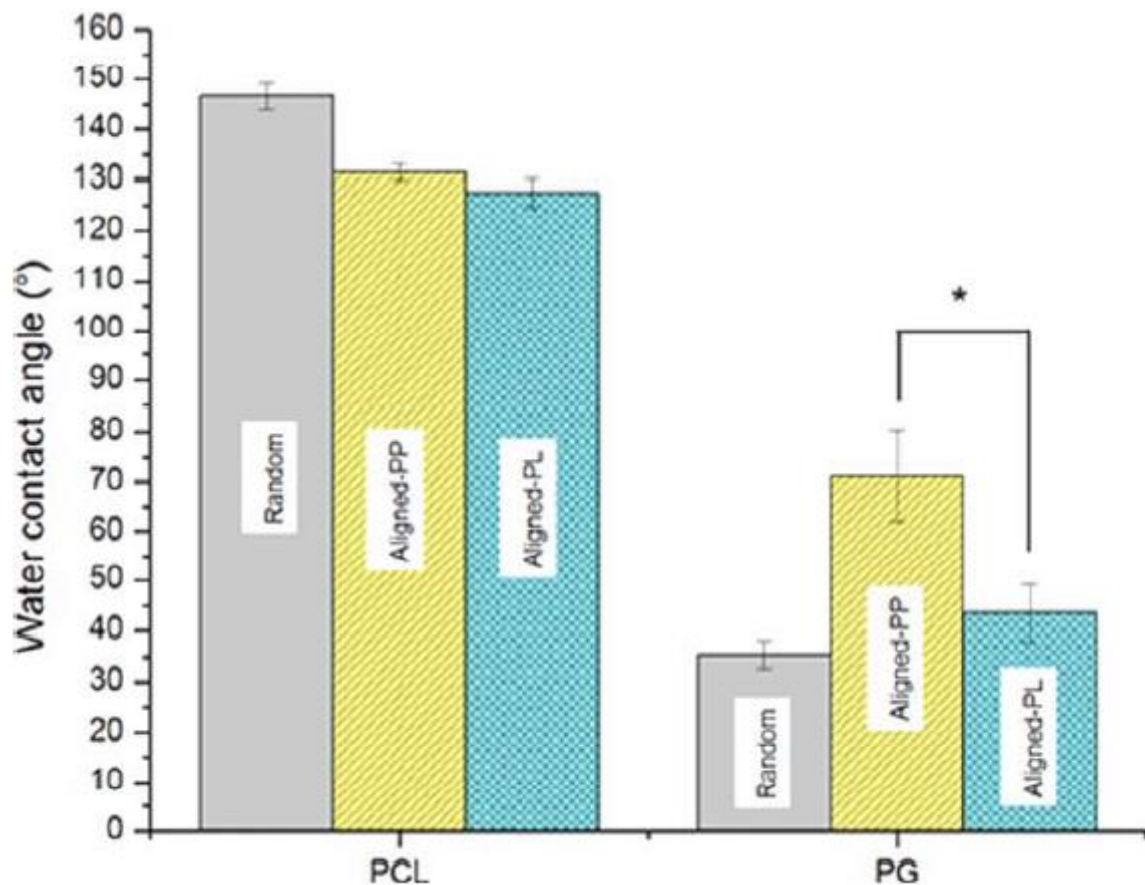


*Fig 4. Water contact angles of random and aligned PCL and PG nanofibers. Contact angles of aligned nanofibers were measured in perpendicular (PP) and parallel (PL) directions. *Significant difference ($p \leq 0.05$) between the contact angle of A-PG in PP direction compared to contact angle along PL direction [21].*

Fibers alignment gave cells a topographical stimulus guiding cells anisotropic organization. The aligned fibers could give feedback to promote the cellular proliferation and differentiation. This was the first study demonstrated that the electrospun fibers with nano-scale alignment was able to direct CM alignment.

Aligned PG nanofibers also provided anisotropic wetting and better mechanical properties for cardiac regeneration than PCL and random PG scaffolds. Cardiomyocytes seeded on aligned PG nanofibrous scaffolds showed higher attachment and greater organization compared with PCL scaffolds.

Raheleh *et al.* [23] studied the effects of random and aligned PCL scaffolds on cardiomyocyte differentiation, particularly the expression of 4 important cardiac-related genes at 3 time points during cardiomyocytes differentiation of adipose stem cells (ASCs) (Fig 5). They performed all experiments in 3 groups including ASCs seeded on aligned and random PCL and tissue culture polystyrene (TCPS) as control. The expression of the 4 genes was higher in scaffolds compared with TCPS [23].

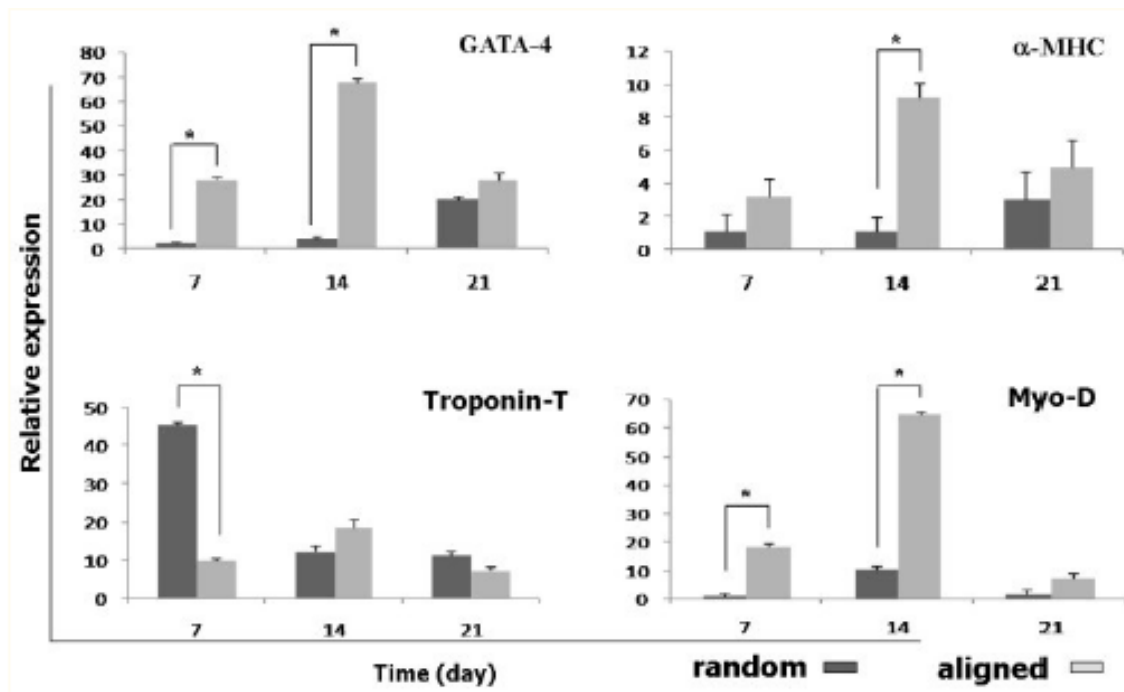


Fig 5. Relative expression of troponin T, GATA-4, Myo-D and α-MHC on days 7, 14 and 21 in the human ASCs during cardiogenic differentiation, asterisk shows significant difference between two groups on each day at $P < 0.05$ [23].

1.7.1) Cell micropatterning for 2D CM alignment

Simpson *et al.* studied the effect of the morphology of the substrate on CMs, these cells were aligned on a thin collagen surface coating that deposited them by a cell scraper, polymerized and poured within a slightly tilted dish [24]. Then, microabrasion was adopted to obtain aligned CMs with anisotropic sarcomeric structure, using unidirectional abrading polyvinyl chloride (PVC) coverslips by lapping papers with different grit sizes [25].

Mathur *et al.* [26] developed a model that provided precise control over cell types, ECM composition, cell-cell interactions, and microenvironment geometry. Lately, microfabrication-based patterning techniques was used as platforms to investigate CMs physiological and pathological features. Microchannels in PDMS was used to guide cell alignment. Cells of different dimension and form was stuck using Microcontact printing ECM protein and creating areas in which the cells adhered on different cell-repelling surfaces such as laminin onto polyacrylamide thin films or fibronectin onto alginate. A lot observations displayed that aligned CMs had behavior more like adult mouse myocardium compared to those cultivated in randomly oriented cultures. However, monolayer of aligned neonatal rat CMs deposited with this technique underwent fibrosis with the activation of TGF- β signaling pathway. Furthermore, interactions between myofibroblasts and CMs could lead to a lowering of electrical conduction.

To increase the maturity level of hiPSC-CM Micropatterning hiPSC-derived CMs (hiPSC-MCs) was used by microcontact printing collagen onto polyacrylamide. A similar approach was used to fabricate a hESC-CM microarrays for drug screening using laminin, in order to evaluate the effects of H_2O_2 treatment on CMs viability and contractility.

Micropatterning techniques allowed to control accurately the size of the cell and their shape. Besides they were used to produce uniform embryoid (EBs) for studies of embryogenesis and cardiomyogenesis. The size of EBs is an important parameter for the differentiation, in fact there was higher endothelial differentiation in small EBs and higher CM differentiation with large EBs contained in poly(ethylene glycol) (PEG).

Another study [27] showed that yield and reproducibility of cardiac differentiation could be improved using microwells in silicone rubber sheets build up with laser cutting.

In research of recent years was discovered that self-organization of hESCs can be activated by the geometric confinement from the micropatterned substrate and this organization summarize spatial cell fate patterning during the development of the embryo. In response to BMP4, colonies reproducibility differentiated to an outer trophoctoderm-like ring, an

inner ectodermal circle, and a ring of mesendoderm expressing primitive-streak markers in between. Self-organizing lineage specification and creation of a 3D beating human cardiac microchamber was encouraged by the correct balance of biochemical input and geometric confinement on micropatterned hiPSCs, which was very similar to the developing primitive human heart. These *in vitro* chambers were used to test suspicious drugs that could lead to malformation during development. An example is thalidomide that provokes a reduction in differentiation efficiency, damages the formation of cardiac microchambers with smaller size, lower contractility, and decreases the beat rate respect to the control.

Micropatterning technique remains a 2D culture support, even if it can regulate the function and the morphology of the cells and it allows high-throughput analysis. Therefore, it cannot reach all the architecture and functional capabilities of a human organ. However, more complex models that can mimic also the 3D structure of the tissues can be achieved from these 2D models. The research on these 2D models is concentrating to develop methods that can allow the characterization of the heterogeneity of cell population, and high-throughput screening for single-cell response to various environmental cues. Single CM micropatterning was used to study myofibrillogenesis and its correlation with extracellular cues. Researchers found that not only cell shape was defined but also cytoskeleton was under reorganization into the predicted architecture, this was discovered by microcontact printing ECM protein on the coverslip to shape single CM into the predesigned patterns. Cell shape, sarcomere orientation, and nuclear morphology was also regulated by the spatial configuration of ECM [28].

1.8) 3D cardiac tissue models

Engineered heart tissues (EHTs) are three-dimensional, hydrogel-based muscle constructs that can be generated from isolated heart cells of chicken, rat, mouse, human embryonic stem cell (hESC) and hiPSC. The method for the generation of EHTs requires (i) heart cells, (ii) a liquid hydrogel that solidifies and promotes tissue formation, (iii) a casting mold that determines the 3D shape of the developing tissue and (iv) a support structure to which the cell-containing hydrogel attaches or that otherwise provides mechanical restraint for the developing heart tissue. The most difficult parameter to set is the orientation and strength of the continuous mechanical input to provide to the cells since they orient and align along stress lines. First embryonic chicken heart cells were reconstituted in collagen I and rectangular casting molds, which were equipped with a pair of Velcro-covered glass tubes

kept on distance by a metal brace and yielded biconcave lattices. In the next studies a circular design of the casting mold was used with neonatal rat heart and a collagen I plus Matrigel mix as hydrogel matrix was used. In this early models EHTs were dipped into organs baths to obtain contractile parameters [29].

1.8.1) 3D matrices production

Zhen et al [30] concentrated on modelling the cardiac tissues affected by the long QT type 3 (LQT3) syndrome. A bioinspired cardiac tissue model with a 3D filamentous matrix was created to regulate the structural alignment of CMs and to adapt the cellular mechanical environment. The developed model was based on the use of Patient specific iPS cell-derived cardiomyocytes (iPS-CMs) and in the study of long QT syndrome (LQTS). In this study an *in vitro* model of three-dimensional (3D) human cardiac tissue was developed by seeding synthetic filamentous matrix with cardiomyocytes derived from healthy wild-type volunteer (WT) and patient-specific long QT syndrome type 3 (LQT3) induced pluripotent stem cells (Ips-cmS) to simulate the human ventricular myocardium. LQT3 cells enhanced late Na^+ channel currents that failed to inactivate completely and conduct increased inward currents. This prolonged depolarization resulted in delayed repolarization, a prolonged QT interval, and increased the risk of fatal arrhythmia. Experiments displayed that CMs differentiated from LQT3 iPS cells had the electrophysiological abnormality of delayed repolarization shown in LQT3 syndrome. A disease-specific 3D cardiac tissue was generated by cultivating LQT3 iPS-CMs on such a highly controllable filamentous matrix and the contractility malfunctions associated to LQT3 syndrome was studied. Several drugs associated with cardiotoxicity were tested on the 3D tissue model created and the results were compared with 2D cell culture. The filamentous matrices were fabricated via the two photon initiated polymerization (TPIP), system based on a femtosecond laser beam irradiated vertically into the photoresist, that is a UV-curable organic-inorganic hybrid polymer. The assembled glass scaffold was filled by uncured photoresist and placed on PX-controllable X-Y-Z motorized stages with high precise positioning. Single fibers were fabricated along the laser beam path with a high-repetition rate femtosecond laser irradiation. Fibers with a diameter of 5 μm and 10 μm were created. By using a PC, it was possible to control the X-Y-Z stage with high positioning precision and so to have different fiber spacing within the matrices.

1.8.1.1) Generation of 3D cardiac tissue

A 6-well plate was used to storage each filamentous matrix. The matrices were rinsed with Dulbecco's phosphate-buffered saline (DPBS) three times and then coated with 50 µg/mL fibronectin DPBS solution for 1 h before loading the cells. Sheets of beating CMs were dissociated using a singularization protocol. The cells were collected, pelleted and resuspended in EB20 MEDIA, 500 µL suspension with a density of 1 million cells/mL was pipetted over each matrix.

1.8.1.2) Characterization of obtained matrices

Two classes of filamentous matrices were designed: (1) constant fiber spacing with varying fiber diameter (5 µm and 10 µm); and, (2) constant fiber diameter with varying fiber spacing (25 µm, 50 µm and 75 µm). To achieve a 3D structure were used three layers of fibers. AFM was used to measure the fiber stiffness as shown in **Tab 1**.

Diameter (µm)	Elastic modulus (MPa)
5	158 ± 9.1
10	598 ± 86

Tab1. Calculated effective elastic modulus of the fibers within the filamentous matrices [30].

1.8.1.3) Characterization of cardiac differentiation

The mTeSR1 medium into Matrigel-coated plates was used to cultivate LQT3 and WT iPS cells. Both kind of cells expressed abundant amount of pluripotent markers as Oct4, Sox2, and SSEA4, confirmed by flow cytometry (**Fig 6A**). One day after passage the LQT3 iPS cells were subjected by immunostaining with antibodies against Oct4, Nanog, and Sox2, they displayed homogeneous expression of these pluripotent markers.

CMs started to beat at Day 8 and developed CMs organized in contracting sheets by Day 10. At day 12, an upregulation of cardiac specific genes NKX2.5, TNNT2, TNNI3, MYH6, and MYH7 on both kind of cells occurred, verified by RT-qPCR analysis. These sheet-beating CMs stained positive for sarcomeric α -actin, cardiac Troponin T (cTnT), and β -myosin

heavy chain (**Fig 6B&C**). The both lines of cells were submitted to flow cytometry and it demonstrated that the differentiation efficiency was about 90% CMs, in LQT3 cell lines, and 75% CMs, in WT cell lines, in the whole cell population(**Fig 6D&E**). These data verified that LQT3 iPS-CMs could reproduce the LQT3 electrophysiological abnormality in vitro.

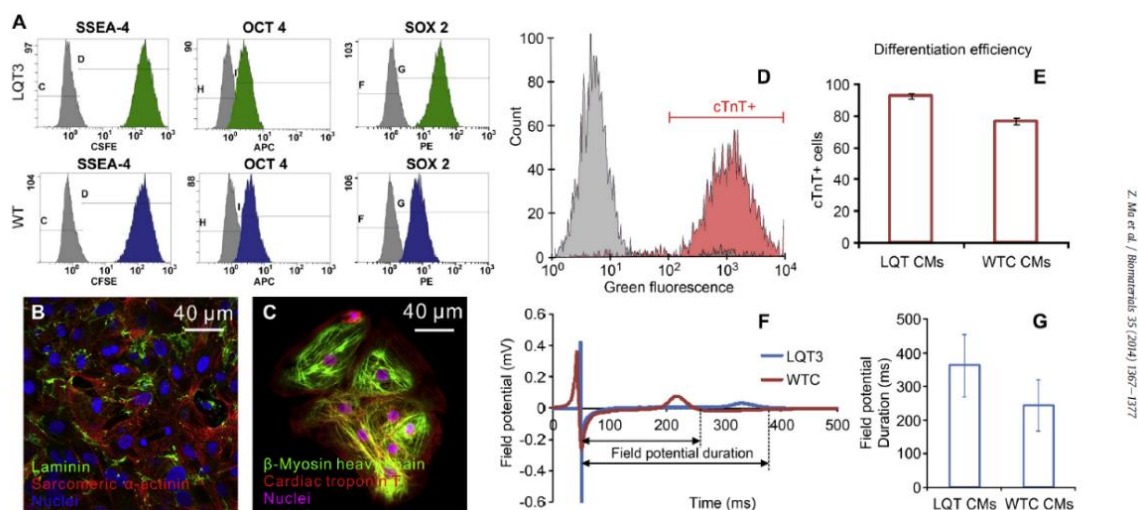


Fig 6. (A) Characterization of LQT3 and WT iPS cells with pluripotent markers SSE4, Oct4, and Sox2 with flow cytometry method. The differentiated LQT3 iPS-CMs expressed cardiac specific markers; (B) sarcomeric α -actin and (C) cardiac Troponin T (CTnT) and β -myosin heavy chain. The differentiation efficiency was characterized using flow cytometry method, and histogram (D) showed that the selected cTnT+ population (red) represented the CMs relative to isotype control (gray). (E) About 90% purity for LQT3 iPS-CMs differentiation and 75% purity for WT iPS-CMs differentiation was obtained. (F) The waveforms of field potentials measured using MEA system were plotted and showed elongated FPD of LQT3 iPS-CMs comparing to WT iPS-CMs. (G) The average FPD for LQT3 iPS-CMs was w370 ms, whereas WT iPS-CMs was w250 ms [30].

1.8.1.4) Drug testing on cardiac model

After the model for LQT3 iPS-CMs was optimized, it was validated by testing the effects to different chemical compounds that have well-known effects on cardiac cells. The model was made to grow with two doses of each compound, then the CMs responses was evaluated by real-time video recording and motion tracking software to assess the contractility malfunctions (**Fig 7**). E4031, a hERG K⁺ channel blocker, and propranolol, a beta-adrenergic antagonist showed similar effects on LQT3 iPS-CMs, decreasing beating frequency (BF) and maximum contractility velocity (MCV) and increasing the beating duration (BD) in a dose-dependent manner. E4031 blocker caused a small level of irregular beating patterns shown in the baseline of the motion-tracking waveform, but propranolol induced significant uncoordinated beating, suggestive of cardiac arrhythmias.

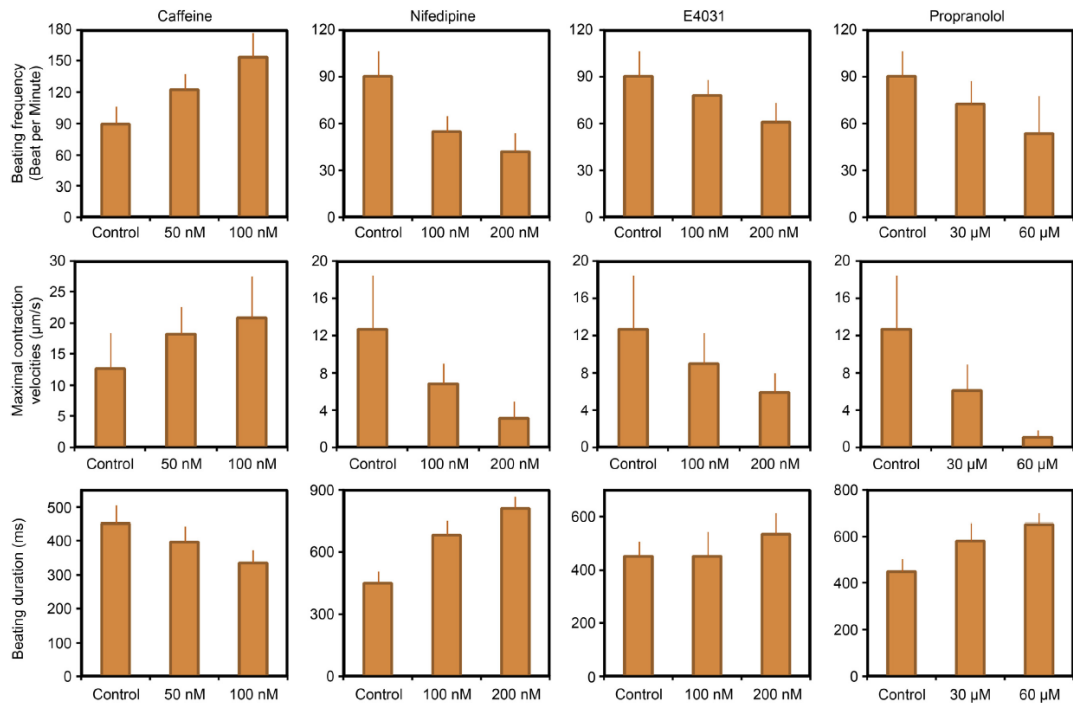


Fig 7. Four different compounds (caffeine, nifedipine (L-type Ca^{2+} channel blocker), E4031 (hERG K^+ channel blocker) and propranolol (b-adrenergic antagonist) were tested on the LQT3 iPS-CMs on F/5-50 matrices. The only compound that augmented the CMs contractility was caffeine, while the other three molecules decreased the contractility at a dose-dependent manner [30].

2) State of art for *in vitro* cardiac model

There are three main steps to design an *in vitro* model. The first is the creation of the scaffold in which the cells are cultivated. The second is the functionalization of the scaffold with a protein that makes it more biomimetic. The decided coating must be also stable and homogeneous, that is why covalent grafting is suggested comparing to the simple immersion of the scaffold in the solution with the chosen protein. The last step is the culture of the desired cells. After the seeding and culturing of cells, the correct technique must be used to understand eventual phenotype changes and mutation and to evaluate cells activity. To do this there are some techniques as the RT-PCR, or the technique of immunochemistry that evaluate the gene expression and the presence of a protein in the culture environment, respectively. The cardiac fibrotic tissue is characterized by an aligned architecture due to the ECM morphology and this orientation is followed by the cells present in the area, such as cardiac fibroblasts and myofibroblasts. This structure is given by the stress generated from the beating of the heart during the first days after the stroke. That is why in our study, another kind of validation is the alignment of the cells.

2.1) Electrospinning models

Orlova *et al.* [31] built an *in vitro* system for cardiac tissue engineering cultivating cardiomyocytes on electrospun polymethylglutamide (PMGI) nanofibrous meshes either imprinted on solid substrate or suspended in space. The solution of PMGI was prepared at 13% in cyclopentanone and tetrahydrofurfuryl alcohol. The ionic surfactant sodium dodecyl sulphate (SDS) dissolved in ethanol was added to the polymer solution with a concentration of 0.48 g/L.

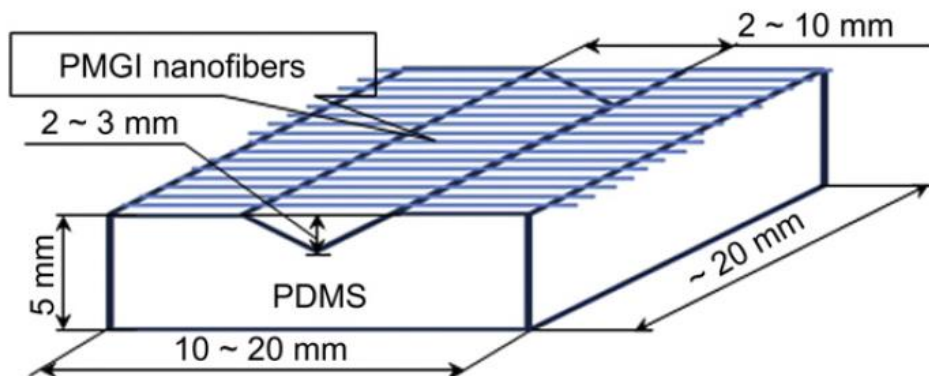


Fig 8. Scheme of PDMS scaffold with suspended PMGI nanofibers [31].

Nanofiber membrane was placed on glass by using the microcontact printing technique. First a layer of Polydimethylsiloxane (PDMS) was made and then it was also used for the suspended PMGI nanofibers (**Fig 8**).

The PMGI fibers were produced applying 8 kV potential between the solution and the grounded collector. The solution was loaded into a 1 mL syringe and delivered through a 25-Gauge blunt-tip needle. The flow rate was set to 2.0 mL/h. The distance between the collector and the tip of the syringe was 10 cm. A circular collector was used to collect random nanofibers. A rectangular hole was created in the collector to ensure the presence of aligned fibers. The obtained fibers were deposited onto PDMS holders and stored under vacuum for 24 h to ensure the complete evaporation of the solvent.

The collected fibers were fastened onto a 22 mm glass cover slip by micro-contact printing before to put them on PDMS substrate. This step was necessary for the preparation of solid substrate covered with PMGI nanofibers for cell seeding since fibers could not adequate adhere on PDMS substrate. Briefly, ethanol-cleansed glass cover slips were kept on a hot plate at 200 °C, which was slightly above the glass transition temperature for PMGI, for 10-30 s. A PDMS holder coated with nanofibers was kept in contact with the hot glass and held for 30 s. After cooling to room temperature, the PDMS holder was detached from the glass surface leaving the imprinted fibers without any alterations. Depending on the length of the PMGI nanofibers, the glass cover slip was either partially or fully covered with nanofibers. Fibers were electrospun from a 13% solution of PMGI polymer in cyclopentanone and tetrahydrofurfuryl alcohol. SEM micrographs displayed random PMGI (**Fig 9a**) and aligned fibers (**Fig 9b, c**).

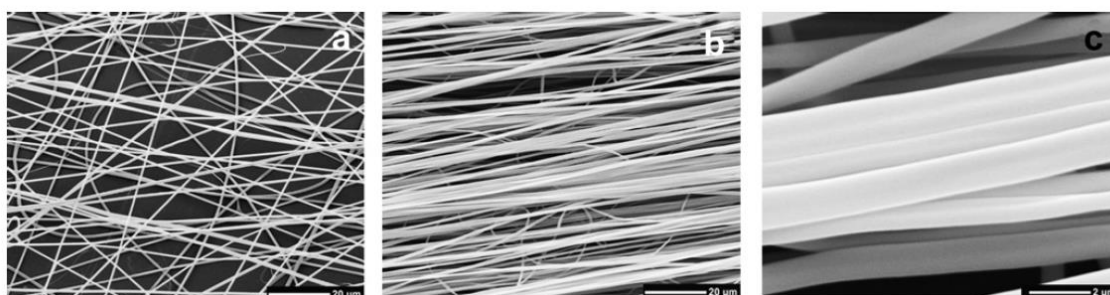


Fig 9. SEM images of electrospun PMGI: (a) random; (b,c) aligned [31].

In the study of Parrag et al. [32] two scaffolds were fabricated, one with unaligned fibers and the other with aligned fibers to study which one give better results. On the scaffolds were cultivated murine embryonic stem cells-derived cardiomyocytes (mESCDCs) co-cultured with mouse embryonic fibroblasts (MEFs). The scaffold was formed by two

polyurethanes. The first PU contained a phenylalanine (Phe)-based diester chain extender, polycaprolactone diol of molecular weight 1250 (PCL1250), and 2,6-diisocyanato methyl caproate and was referred to as the Phe PU. The second PU was by Gly-Leu-based chain extender. The two PU was dissolved in dichloromethane at concentrations of 14% and 10% (w/v) concentrations for the first and second PU respectively. The solution was loaded into a 22-Gauge syringe and the syringe pump was set to 6 mL/h using a voltage power supply of 12 kV.

Random fiber scaffolds were produced using a rotating mandrel and translating at 5 cm/s. The rotation of mandrel was increased to 270 cm/s to collect aligned fibers.

Hussain et al. [33] prepared an 8% (w/v) chitosan solution by dissolving chitosan in Trifluoroacetic acid. The solution was stirred overnight at 40 °C. Methylene Chloride was added to form a final volume to volume ratio of 80:20. The chitosan solution was fed into a 10 mL disposable syringe fitted with an 18-gauge needle. A voltage of 30 kV was applied between the tip and the collector to electrospinnate the solution. The distance between the collector and the needle was set at 30 cm and the flow rate was 2 mL/h. After the vacuum drying at room temperature, the chitosan nanofibers were cut into pieces to fit into 35-mm dish and neutralized with 15N ammonium hydroxide: 100% ethanol (1:1 v/v ratio) for 30 min. The chitosan nanofibers were then washed with distilled water three times for 15 min each time. The chitosan nanofibers were then sterilized under a UV lamp for 20 min. On the scaffold were cultivated neonatal rat cardiomyocytes.

2.2) Coating strategies for cardiac cells culture

The majority of materials used for scaffold fabrication need to be improved in their cell-interactive properties. This can be achieved by grafting some specific molecule on the surface or the bulk of the scaffolds. There are different kind of surface modification techniques to conjugate chemically bioactive functional groups on substrates, such as chemical surface etching with HCl or NaOH, plasma treatment and gamma-ray irradiation. Biomolecules as fibronectin, gelatin, collagen, Arg-Gly-Asp (RGD), and Tyr-Ile-Gly-Ser-Arg (YIGSR) peptide can be graft on surface by using acrylic acid (AAc) and acrylamide (AAM) and creating carboxyl and amine groups on which link the biomolecules [34].

2.3) Coating with a layer of Polydopamine

Polydopamine was used recently as a biomimetic adhesive coating for different materials. The adhesive characteristic of this molecule is given by catechol and amine groups present in its chemical structure. Dopamine polymerized and created thin layers on the surface of different materials such as metals, ceramics or polymers by oxidation at adjusted alkaline pH to form dopamine-quinone.

In the study of Shin *et al* [35] dopamine was polymerized on the surface of electrospun poly(L-lactide-co- ϵ -caprolactone) (PLCL) fibrous matrices. First the matrices were dipped in 70% ethanol and distilled water (DW), then it was immersed in the dopamine solution (2mg/mL in 10 mM Tris-HCl buffer, pH 8.5), and then shaken on the rocker for 30 min at room temperature. After the reaction, the matrices were washed with DW three times to remove unreacted or aggregated dopamine, and the polydopamine coated matrices were stabilized at 50 °C for 2 h (D-PLCL). Mechanical properties of the matrices were tested with a universal testing machine.

The polydopamine coated PLCL fibrous matrices were dipped in gelatin solution (0.2 or 2 mg/mL in Tris-HCl buffer) and shaken on a rocker for 30 min at room temperature. After incubation for 2 h at 50 °C, residues of gelatin were then washed out with DW under vigorous shaking for 12 h.

The surface modification of electrospun fibrous matrices using polydopamine was achieved, as shown in **Fig 10**. SEM images were taken to observe the morphology of the electrospun fibrous matrices before and after the modification processes. PLCL fibrous matrices had random fibrous structure with high porosity (**Fig 10**), the average diameter of fibers had a ranged from 700 nm to 1.2 μ m. The structure of the fibers was not affected by the polydopamine coating. The change in color on the D-PLCL fibrous matrices displayed the homogenous coating of polydopamine.

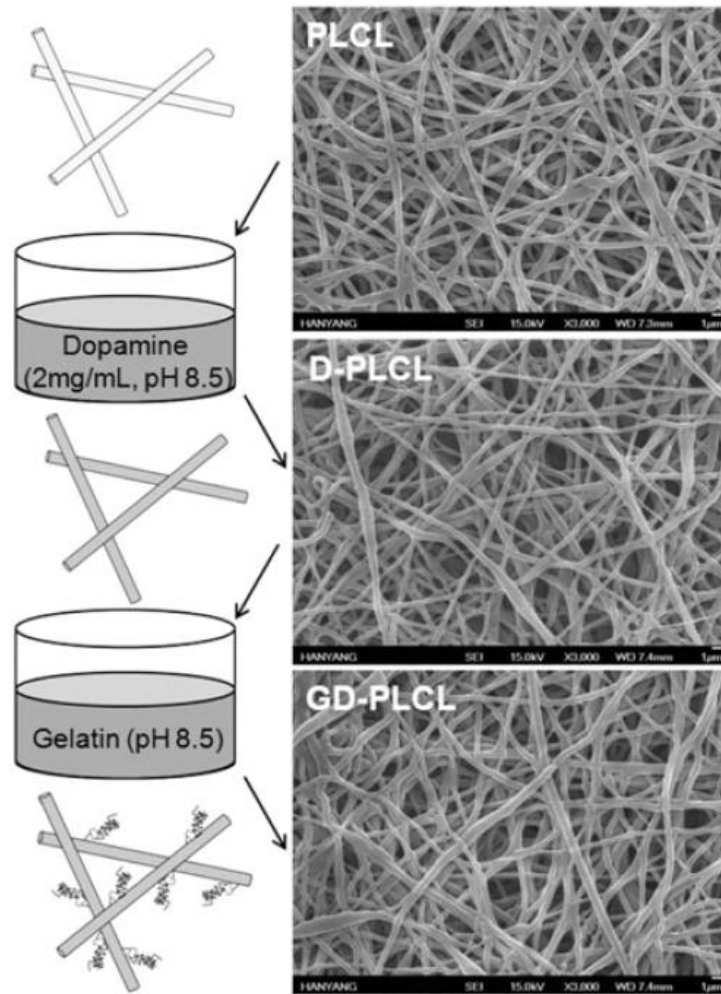


Fig 10. Scanning electron microscopy (SEM) images of PLCL fibrous matrices with gelatin immobilized on polydopamine coating [35].

The cells used in the study were H9c2 myoblasts. After 24 h of incubation, the number of adherent cells on the PLCL, G-PLCL, D-PLCL, and GD-PLCL were 26 ± 7 , 37 ± 11 , 52 ± 11 , and 63 ± 15 , respectively (**Fig 11**). It was calculated that the spreading area of a single cell was 345.5 ± 86.4 and $391.6 \pm 122.1 \mu\text{m}^2$ on the PLCL and G-PLCL matrices, while for D-PLCL and GD-PLCL scaffolds were 621.1 ± 76.1 and $763.0 \pm 99.8 \mu\text{m}^2$, respectively (**Fig 12**). After 5 days H9c2 myoblast proliferation was higher on the GD-PLCL matrices, as compared to the other matrices (**Fig 13**). The DNA content on the GD-PLCL (468.8 ± 11.1 ng) matrices at 1 day was greater than that on the PLCL (348.2 ± 30.4 ng), G-PLCL (345.9 ± 27.5 ng), and D-PLCL (377.6 ± 24.9 ng). BrdU analysis was carried out to assess the

proliferation of H9c2 myoblasts on the fibrous matrices. Proliferation on the D-PLCL and GD-PLCL was greater than the other groups (**Fig 14**).

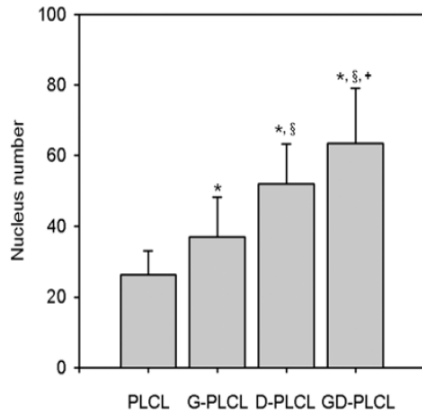


Fig 11. Average number of adherent H9c2 myoblast cells on the fibrous matrices. Asterisk “*” indicates statistical significance relative to the PLCL fibrous matrices, “§” relative to the G-PLCL fibrous matrices, and “+” relative to the D-PLCL fibrous matrices ($p < 0.05$) [35].

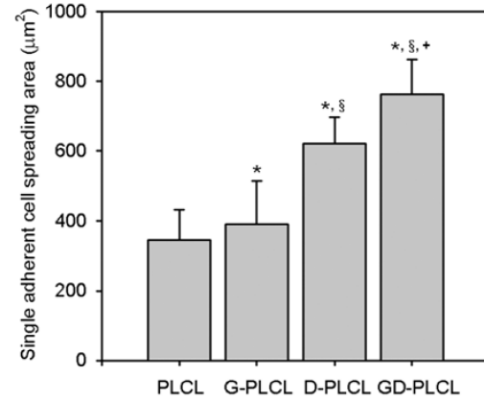


Fig 12. The single adherent cell spreading area on the fibrous matrices. Asterisk “*” indicates statistical significance relative to the PLCL fibrous matrices, “§” relative to the G-PLCL fibrous matrices, and “+” relative to the D-PLCL fibrous matrices ($P < 0.05$) [35].

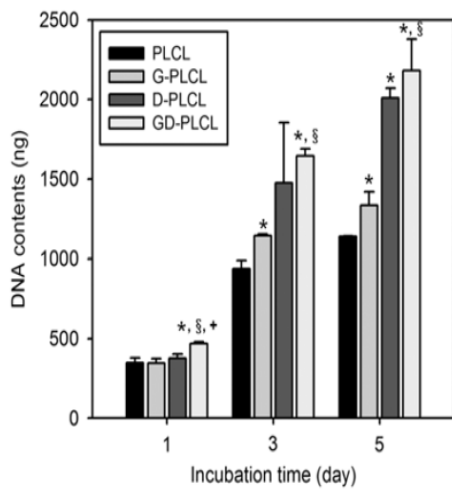


Fig 13. Proliferation of H9c2 myoblast cells cultured on the fibrous matrices. Asterisk “*” indicates statistical significance relative to the PLCL fibrous matrices, “§” relative to the G-PLCL fibrous matrices, and “+” relative to the D-PLCL fibrous matrices ($p < 0.05$) [35].

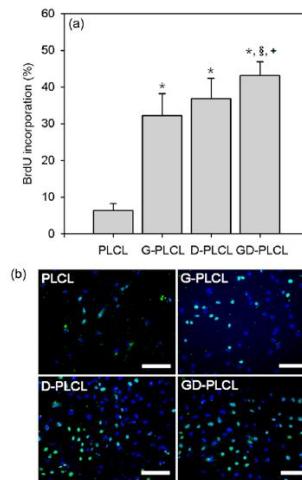


Fig 14. (a) Relative BrdU incorporation of H9c2 myoblast cell cultured on the fibrous matrices and (b) representative images of BrdU incorporated cells. Nucleus were stained in blue and anti BrdU were stained in green. Asterisk “*” indicates statistical significance to the PLCL fibrous matrices, “§” relative to the G-PLCL fibrous matrices, and “+” relative to the D-PLCL fibrous matrices ($p < 0.05$) [35].

2.4) Plasma grafting and plasma treatment

Plasma grafting and plasma treatment are effective methods for surface modification. They allow to select different molecules to link on a material depending on the needed properties. Plasma strongly interact with surfaces bringing chemical and physical modifications through electrons, ions, radicals and neutral molecules creating functional groups on the surface such as amine or carboxyl groups. It was demonstrated that plasma treatment has effects only on the surface leaving the bulk structure intact, even if high-density chains are grafting.

Created functional groups can be used to covalently binding other functional groups.

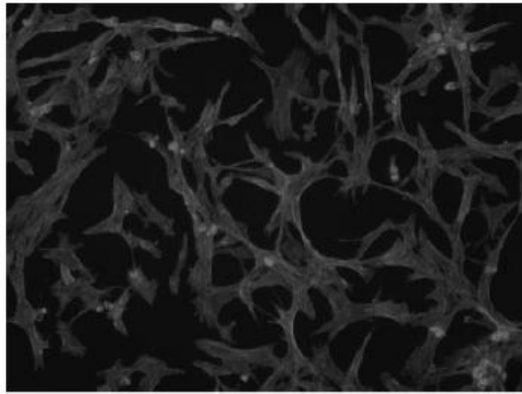
The chemical bonds created with this technique between surface and linked functional groups are more stable and durable respect to the grafting created with physical coating. Plasma grafting is a precise method that concentrates on a precise area and to a depth from some hundred Angstroms to 10 mm [34].

Brown *et al* [36] modulated cell adhesion, myofibrillogenesis and cell cycle progression in neonatal rat ventricular myocytes (NRVMs) by functionalizing a scaffold with ECM protein. These signals were primarily transduced by integrins which mediate adhesion, regulate cellular phenotype, promote migration, signal transduction, programmed cell death, and tissue repair and remodeling. These phenomena increased by reactive hydroxyl and carboxyl groups, that augmented surface energy and wettability through glow discharge.

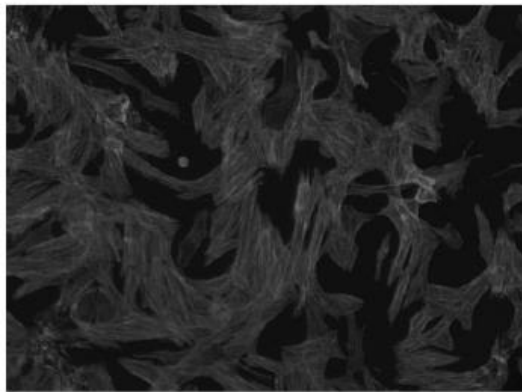
ECM-based surface modification strategies also induced cardiomyocytes to synthesize additional ECM molecules which further promoted morphological transition and myocardial hypertrophy.

Glow discharge involved radiofrequency ionization of inert gases to produce plasma that removed hydrocarbon contaminants, producing an ultraclean and sterile surface. These changes improved protein absorption kinetics. Cell adhesion seemed to be optimal on surfaces with intermediate wettabilities.

In this study was used plasma grafting of acrylic acid on PLGA followed by activation of carboxylic groups by 1-ethyl-3-(3-dimethylaminopropyl) carbodiimide (EDC) and N-hydroxysuccinimide (NHS) for the coupling of fibronectin.

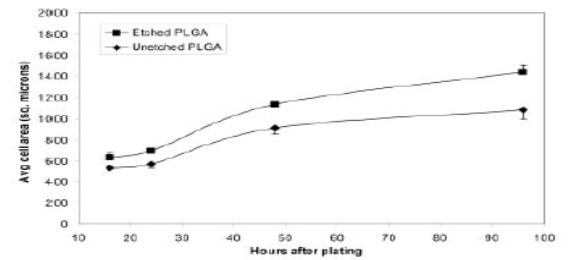


(a)

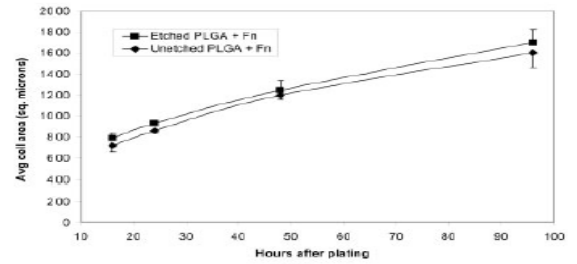


(b)

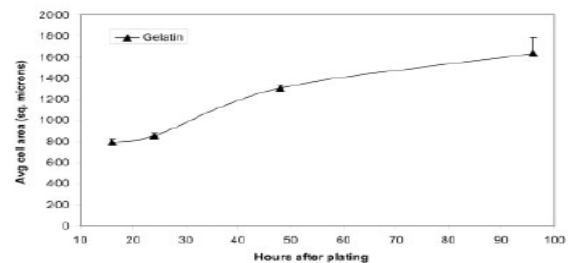
Fig 15. NRVM images on (a) unetched, and (b) etched PLGA after 48 h. Images displayed the increased spreading and myofibril organization on etched films [36].



(a)



(b)



(c)

Fig 16. Image analysis of cell spreading on (a) PLGA, (b) fibronectin-coated, PLGA, and (c) gelatin-coated TCPS. Six DAPI and phalloidin image pairs captured from two culture wells are represented. $P < 0.05$ between all data points with etched and unetched PLGA without fibronectin. $p < 0.05$ between unetched and etched films after 16 and 24 h with fibronectin [36].

It was seen that etching films induced an increase in NRVMs spreading and myofibril organization, which are two characteristics of myocardial hypertrophy (**Fig 15**). If fibronectin was used as coating the etching had less effect. Quantitative image analysis displayed greater spreading by glow discharge (**Fig 16a**) and a reduced effect with fibronectin (**Fig 16b**). Cell spreading increased over plating time on all surfaces, like that observed on gelatin (**Fig 16c**).

The gene expression was measured by using ANF and β -MHC primers linked to fluorescent probe. It was seen that there was a stronger hypertrophic response in NRVMs cultured on etched films respect to unetched films, but when fibronectin was added the effect was high enough to overcome the effect of etching on gene expression.

Boffito *et al* [37] functionalized a round shaped PU films and scaffolds (6 mm in diameter) with gelatin type A and mouse LN1 using a two-step plasma treatment on which they seeded cardiac progenitor cells (CPCs). First the samples were treated with Argon plasma (50 W, 0.7 mbar, 20 sccm) for 5 min to create radical species on the surface. Then, they were immediately subjected to acrylic acid plasma treatment (50 W, 0.05 mbar, 45 sccm) for 15 min to graft and polymerize acrylic acid on the surface, enriching the surface with -COOH groups. These functional groups were utilized for the covalent grafting of G and LN1.

Samples were dipped in an aqueous solution (pH 5.0) containing 5 mg/mL of 1-ethyl-3-(3-dimethylaminopropyl) carbodiimide (EDC) and 1.25 mg/mL of N-hydroxysuccinimide (NHS) at 4°C for 20 h. Scaffolds were then washed 3 times with deionized water (DIW). Finally, LN1 and G were covalently grafted on previously activated sample.

The difference in wettability among scaffolds was evaluated with contact angle (**Fig 17A**). PU films displayed a contact angle of $89.1 \pm 0.1^\circ$. The surface treated with acrylic acid plasma treatment had a static contact angle $48.6 \pm 1.5^\circ$ confirming the grafting with hydrophilic acrylic acid functionality. The contact angle after grafting with G or LN1 increased to $61.3 \pm 2.1^\circ$ and $66.3 \pm 0.8^\circ$, respectively, showing no remarkable differences.

Then Toluidine Blue O (TBO) colorimetric assay proved the presence of -COOH groups on the plasma-treated surface due to acrylic acid plasma treatment since it showed an intense blue color associated with elevate -COOH density respect to non-functionalized scaffold (**Fig 17B**). Scaffold functionalization with LN1 was analyzed by ELISA assay (**Fig 17C**).

Confocal image analysis revealed that the cells stretched out in three dimensions, among the fibers in the same and in the adjacent scaffold layers. At each culture time, SEM micrographs (**Fig 18A, 18B, 18C, 18D, 18E and 18F**) showed higher cell engraftment on PU-G and PU-LN1 scaffolds vs PU scaffold. After 14 days, cells spread on the scaffold filaments completely filling the pores.

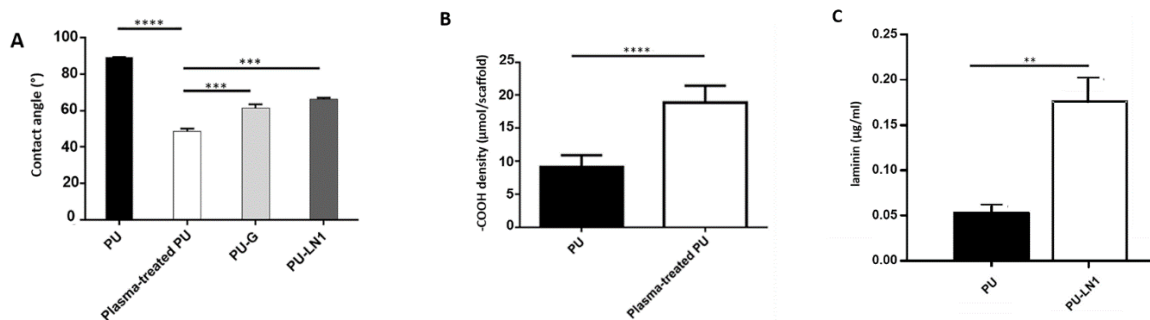
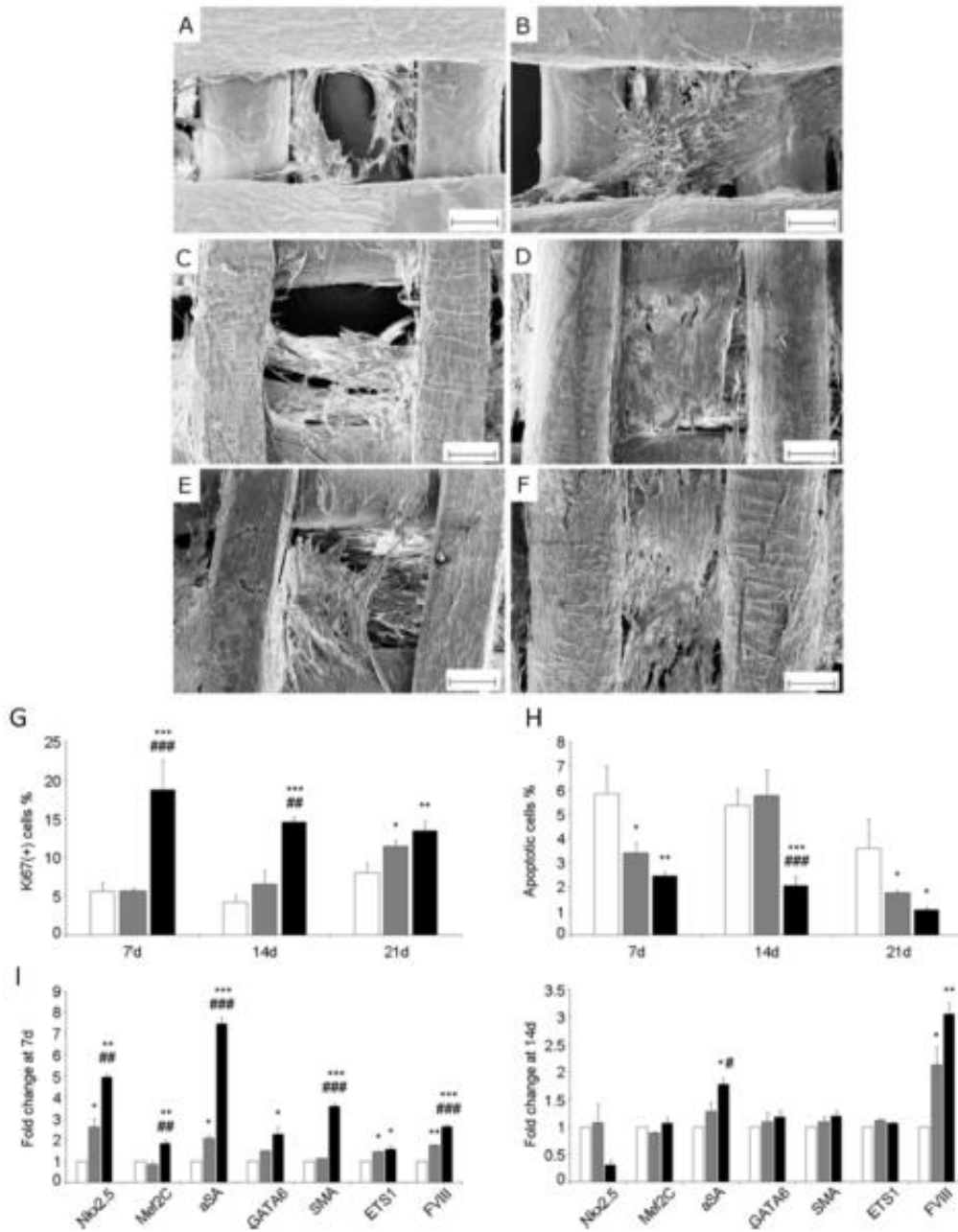


Fig 16. Analysis on scaffolds: (A) contact angle, (B) TBO and (C) ELISA assay [37].

Proliferation of CPCs on PU, PU-G and PU-LN1 scaffolds was assessed by identifying and quantifying actively cycling ki67-positive cells. It was demonstrated that the functionalization with LN1 had the best results both in terms of proliferation and apoptosis.



*Fig 18. SEM images of PU-based scaffolds cultured with human CPCs after 7 and 14 days: (A, B) PU, (C, D) PU-G, (E, F) PU-LN1. Scale bar: 100 μm. (G) Proliferation, (H) apoptosis and (I) gene expression of CPCs on PU scaffolds (control, white bar), PU-G scaffolds (grey bars) and PU-LN1 scaffolds (black bar) at different points. * $p < 0.05$, ** $p < 0.01$, *** $p < 0.001$ vs PU-G scaffolds [37].*

The effect of scaffold functionalization on CPC differentiation was evaluated through the expression of typical markers of primitive cardiomyocytes (MEF2C, α SA), endothelial cell (ETS1, FVIII) and smooth muscle cell lineages by Real-Time Quantitative Reverse Transcription-Polymerase Chain Reaction (RT-PCR) (**Fig18I**). PU functionalized with LN1 gave best results at 7 days. At 14 days the differences started to decrease since differentiation of cells went on with a minus rate.

2.5) Model validation strategies

Parrag et al [32] validated their model by characterizing cell organization, morphology, sarcomere formation, and protein expression determining the differentiated phenotype of the murine embryonic stem cells-derived cardiomyocytes (mESCDCs). In fact, both mESCDCs and MEFs were positively stained for the actin cytoskeleton (red) and cell nuclei (blue), but only the mESCDCs formed sarcomeric structures (green). Constructs were stained for the actin cytoskeleton (f-actin), cell nuclei, and sarcomeric structure (α -actin) 6 days after mESCDC seeding (**Fig 19**).

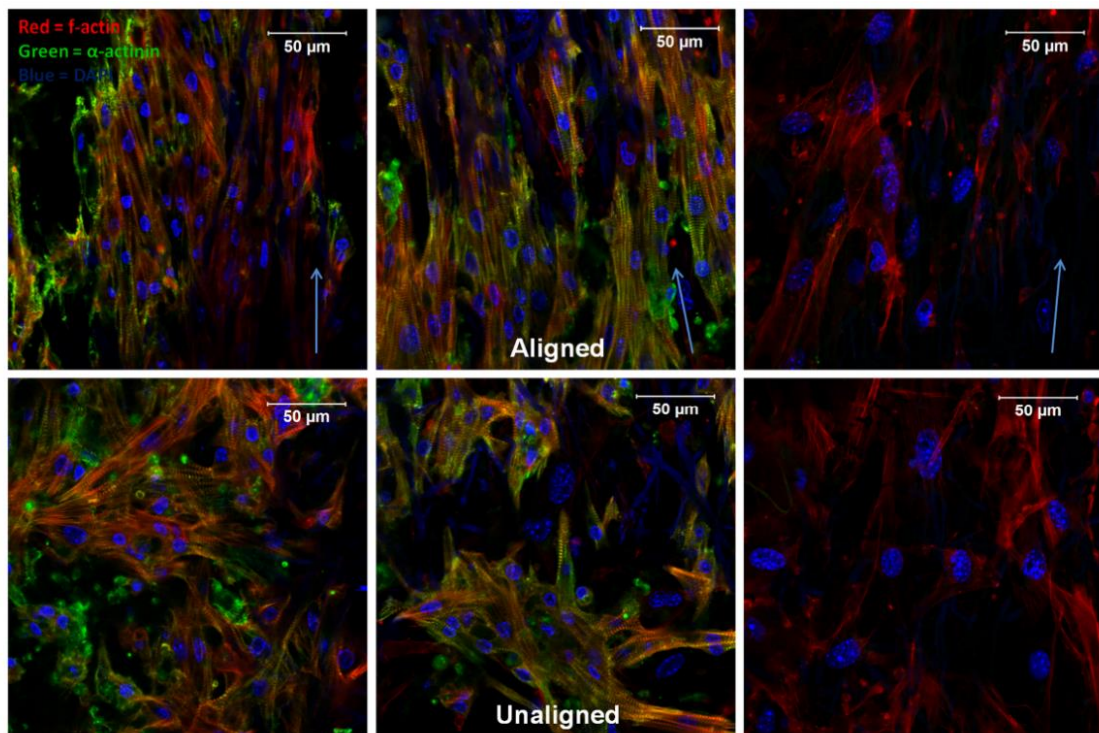


Fig 19. Confocal microscopy images show high-density patches of immunostained cells on aligned (top) and unaligned (bottom) PU scaffolds after 6 days that mESCDCs were seeded. It is displayed the effect of scaffold architecture and coculture on cell morphology and orientation. Red, cytoskeleton (f-actin); green, sarcomere (α -actin); blue, cell nuclei (DAPI); blue arrows, fiber orientation. Scale bars represent 50 μ m [32].

It was seen that the cultured mESCDCs tended to follow the direction of the fibers of the scaffold. The **Fig 20** showed the orientation adopted by the cells in the two different scaffolds. On the aligned architecture most percentage of mESCDCs had a cell angle within the range of $\pm 20^\circ$ from a reference line when cultured alone and with MEFs. Instead the mESCDCs cultured on the unaligned scaffold displayed no general organization. By calculating the standard deviation of the orientation of the cells has been seen that cells on the unaligned scaffold alone and in coculture had a higher mean standard deviation than the same cell group on the aligned scaffold (ANOVA, $P < 0.05$).

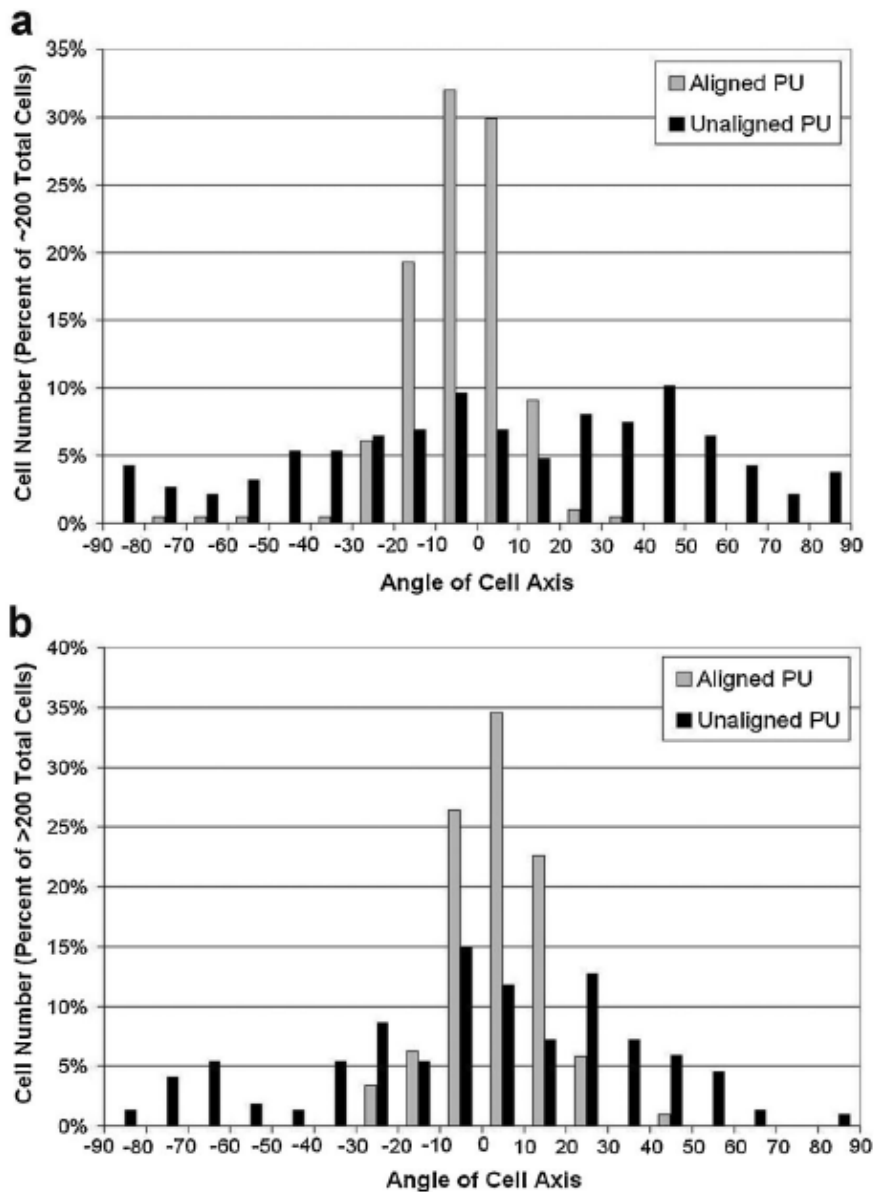


Fig 20. Quantifying the angle of mESCDCs cell axis demonstrates a difference in anisotropic organization of mESCDCs cultured (a) alone and (b) in coculture with MEFs on microfibrillar PU scaffolds. In both cell conditions, the majority of mESCDCs on aligned scaffolds were within $\pm 20^\circ$ of a reference angle. Cells on the unaligned scaffolds exhibited no general organization [32].

A higher number of mESCDCs tended to have a rot-shaped morphology in the aligned architecture respect to those cultivated on unaligned scaffold. Cells cultivated on the aligned fiber scaffold had displayed sarcomeric structures with a cross-striated pattern perpendicular to the major cell axis. On the other side the shape and organization of the cells was variable and mixed. The cocultured constructs showed greater percentage of mESCDCs with a striated myofibrillar structure ($\pm 70\%$) compared to the constructs with mESCDCs cultured alone ($\pm 45\%$; Table I; ANOVA, $P < 0.05$) sign of an improved sarcomere formation by fibroblasts.

Hussain *et al* [38] created a model by using an electrospun scaffold functionalized with fibronectin. They cultured cardiomyocyte alone and in co-culture with fibroblasts.

α -sarcomeric actin (SM-actin) and connexin-43 (Cx43) staining was used to monitoring the cardiomyocyte morphology and gap junction formation, respectively. They were examined on both fibronectin adsorbed chitosan films (2D) and fibronectin adsorbed chitosan nanofibers (3D) both in mono-cultures (cardio-myocytes only) and co-cultures (cardiomyocytes-fibroblasts or cardiomyocytes-endothelial cells).

In the 2D systems, the adhesion of cardiomyocytes mono-culture was poor (**Fig 21A and D**), in fact, the cells displayed low expression of SM-actin and they had a round shape. The minimum of the expression of gap junction protein Cx43 was in the mono-culture system. Instead the co-culture with fibroblasts showed spread morphology and the expression of SM-actin was high (**Fig 21B and 21E**). The peak of Cx43 expression was reached in the fibroblast co-culture. This condition allowed cardiomyocytes to contract in a tissue-like manner in synchronized way. The cardiomyocytes co-cultures with endothelial cells (**Fig 21C and F**) assumed a round-shape morphology with levels of SM-actin and Cx43 expression lower than in the fibroblast co-culture and besides they isolated contractions.

The center of the study was the evaluation of the chitosan nanofibers as a possible tissue engineering scaffold. To do that both cardiomyocyte mono-culture and co-culture were performed on the prepared 3D scaffold and the expression of SM-actin and Cx43 was assessed. The expression of these two markers was not visible in cardiomyocyte mono-culture (**Fig 22A and D**) and co-culture with endothelial cells (**Fig 22C and F**). While cardiomyocyte-fibroblast co-culture had highest expression of the two proteins and a rot-shape networks of contracting cardiomyocytes (**Fig 22B and E**).

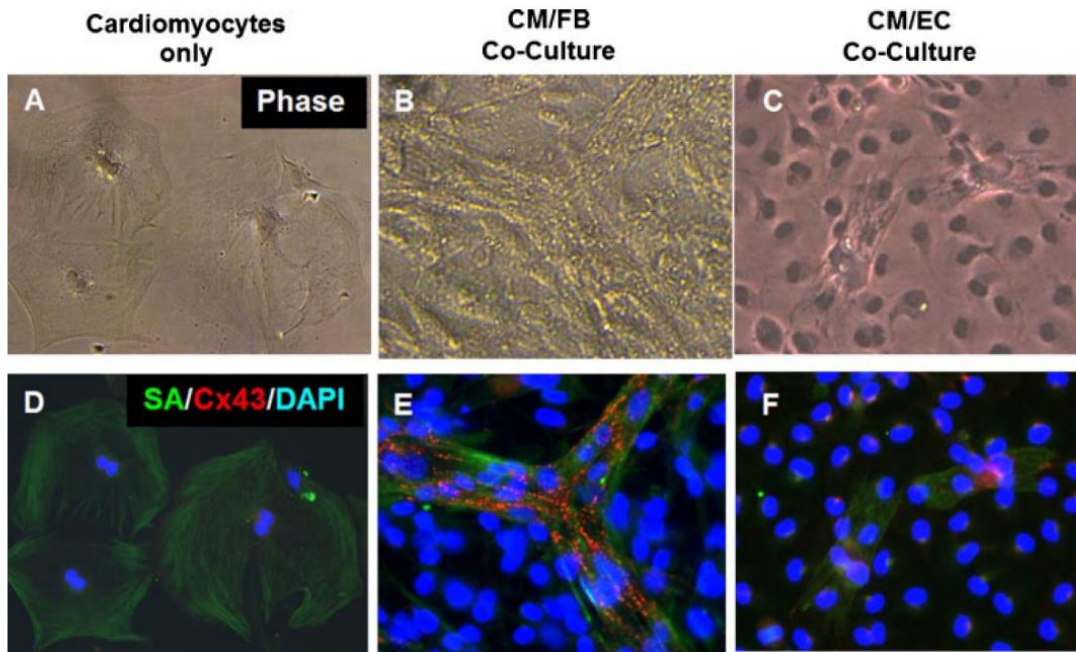


Fig 21. Morphology and phenotypic characteristics of cardiomyocytes on 2D Chitosan-FN film. (A, D): Cardiomyocytes cultured alone, (B, E) cardiomyocytes cocultured with 3T3-J2 fibroblasts, and (C, F) cardiomyocytes co-cultured with microvascular endothelial cells after 7 days of culture. Cardiomyocytes were immunostained for α -sarcomeric actin (SA-actin) and connexin-43 (Cx43) gap junction expression. Neonatal cardiomyocytes (CM), 3T3-J2 fibroblasts (FB), microvascular endothelial cells (EC), 200x original magnification [38].

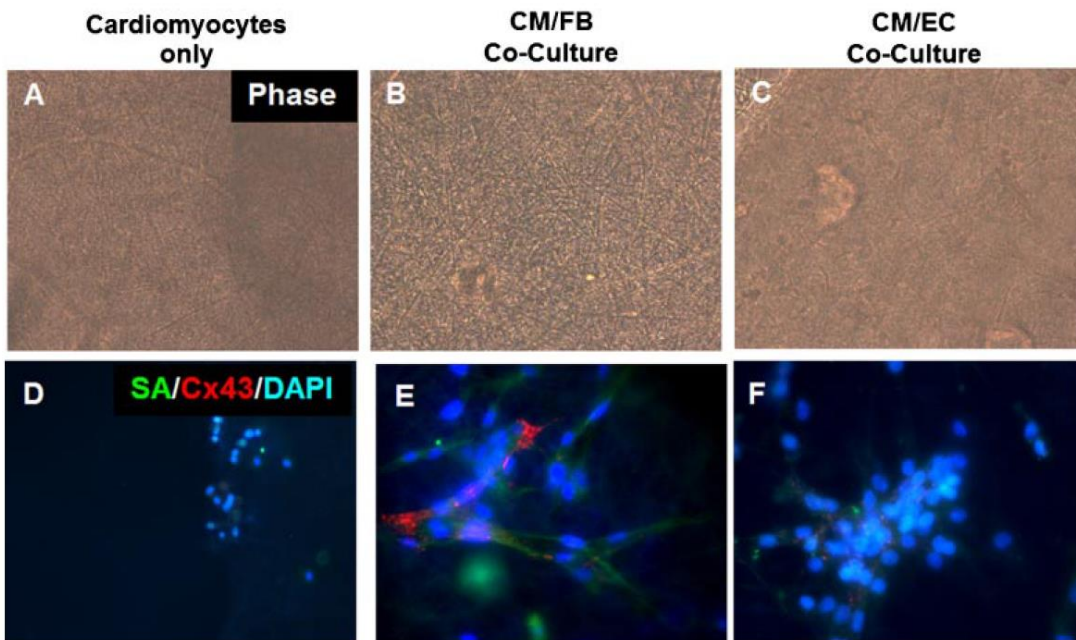


Fig 22. Morphology and phenotypic characteristics of cardiomyocytes on 2D Chitosan-FN film. (A, D): Cardiomyocytes cultured alone, (B, E) cardiomyocytes cocultured with 3T3-J2 fibroblasts, and (C, F) cardiomyocytes co-cultured with microvascular endothelial cells after 7 days of culture. Cardiomyocytes were immunostained for α -sarcomeric actin (SA-actin) and connexin-43 (Cx43) gap junction expression. Neonatal cardiomyocytes (CM), 3T3-J2 fibroblasts (FB), microvascular endothelial cells (EC), 200x original magnification [38].

The samples were dipped in PBS and fixed with 4% paraformaldehyde for 20 min at room temperature for the immunocytochemistry test. Then they were permeabilized in 0.2% Triton X-100 in PBS for 10 min. Then they were washed with PBS and incubated in blocking buffer for 30 min. The primary antibody (mouse anti- α -sarcomeric actin and rabbit anti-connexin 43) was added and incubated for 60 min at room temperature. The samples were washed with PBS and incubated with secondary antibody (donkey antimouse IgG, alexa fluor 488, and donkey anti-rabbit IgG, alexa fluor 594) for 60 min. The samples were stained for 1 h at room temperature with rabbit antifibronectin to assess the absorption of fibronectin on chitosan. Viability of cells cultivated on scaffolds was evaluated by a live/dead viability/cytotoxicity kit and observed with fluorescence microscopy.

Calcium indicator, fluo-4 AM, was used to observe calcium ion flux of beating cardiomyocytes. The stained cardiomyocytes were visualized by fluorescence microscopy.

Fig 23 showed the pseudo color time-frame images of the 3D cardiomyocytes co-culture system. Cardiomyocytes co-cultured with fibroblasts showed rot-shaped morphology and a rhythmic change in intracellular calcium ion concentrations with a frequency of 17 ± 3 contractions per minute. While mono-cultures of cardiomyocytes lost their functionality after 4 days of culture (data not shown).

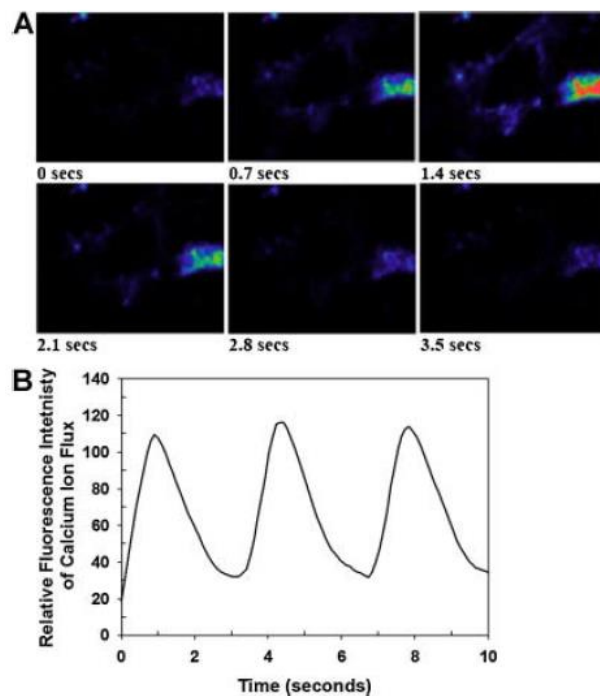
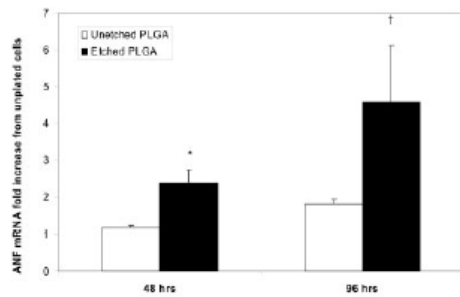
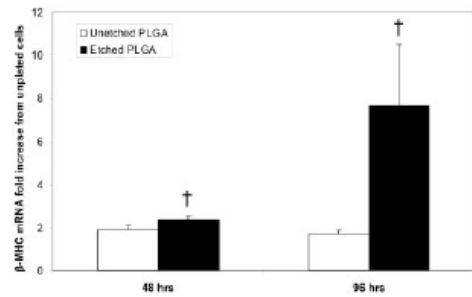


Fig 23. Intracellular calcium ion flux of beating cardiomyocytes in 3-D coculture of cardiomyocytes and fibroblasts after 7 days of culture. (A): Pseudo-color images of calcium ion changes in fluorescence intensity, monitored after 0.7-s time intervals with fluo-4, AM indicator. 200x original magnification. (B): frequency of intracellular calcium ion flux in the 3-D co-cultured. The fluorescence images of calcium ion flux were pseudo-colored, with red representing high calcium ion concentrations and blue representing low calcium ion concentration [38].

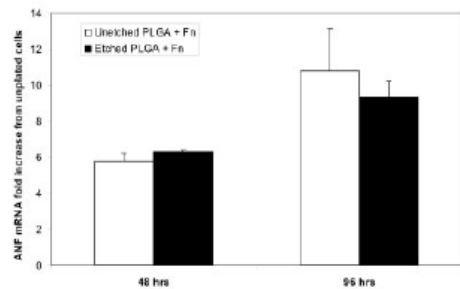
Real-time reverse transcriptase (RT)-PCR system allowed to evaluate the gene expression of the cells under culture. RNeasy was used to isolate total RNA by lysing cells, then QiaShredder columns were used to homogenize, and proceeding through isolation. UV light absorption at 260 nm was used to determine RNA concentration in the purified sample and to approximate the quantity of template in the polymerase chain reaction (PCR) [36]. TAMRA at the 3' end and FAM, VIC and TET at the 5' end were utilized to modified fluorescent TaqMan probes for glyceraldehyde-3-phosphate dehydrogenase (GAPDH), ANF, and β -MHC, respectively.



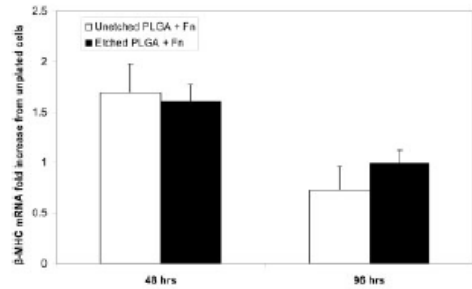
(a)



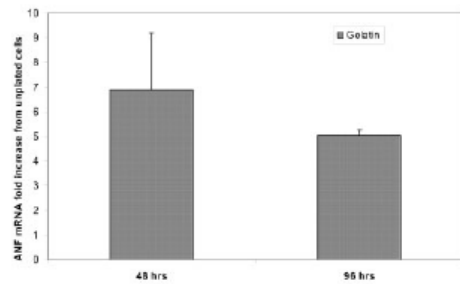
(a)



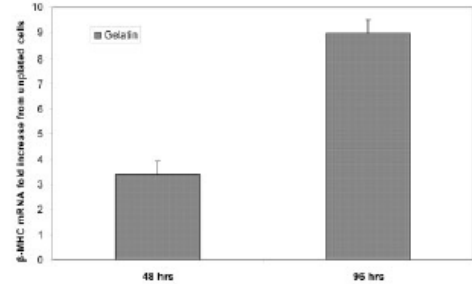
(b)



(b)



(c)



(c)

Fig 24. ANF mRNA expression of NRVMs cultured on (A) PLGA, (B) fibronectin-coated PLGA, and (C) gelatin-coated TCPS. Results were normalized to GAPDH levels and calibrated to expression levels of freshly harvested, unplated NRVMs (mean + SD). Each bar represents measurements from three independent wells measured in duplicate (* $p < 0.05$; $tp < 0.10$ vs unetched PLGA) [36].

Fig 25. β -MHC mRNA expression of NRVMs cultured on (A) PLGA, (B) fibronectin-coated PLGA, and (C) gelatin-coated TCPS. Results were normalized to GAPDH levels and calibrated to expression levels of freshly harvested, unplated NRVMs (mean + SD). Three independent cultures measured were displayed in duplicate in each bar ($tp < 0.10$ vs unetched PLGA) [36].

Comparative threshold cycle method was used to quantify amplification data and relative expression of the target gene was normalized to both GAPDH expression and target gene expression in cells (**Fig 24-25**).

This test displayed that the expression of ANF was higher of two- to three-fold in etched films respect to unetched films. These data indicated that there was a stronger hypertrophic response (Fig 17a), but the etched effect was masked by the adding of fibronectin (Fig 17b). β -MHC was high on etched scaffold (Fig 18a) and there were not remarkable differences with the addition of fibronectin (Fig 18b). These data displayed that fibronectin had more effect than etching on gene expression.

Orlova *et al* [39] developed an *in vitro* system to demonstrate the potential of electrospinning to control cardiac tissue culture architecture. For this purpose, they grew cardiac cells on a polymethylglutarimide (PMGI) electrospun nanofiber scaffold. Cardiomyocytes were isolated from the ventricles of 1-3 day old neonatal Wistar rats using enzyme digestion with collagenase type I.

The samples were fixed in 4% paraformaldehyde for 15 min and washed with PBS three times for 5 min each. The cell membrane was permeabilized by incubation in 0.1% Triton 100 in PBS for 10 min followed by incubation in 1% BSA in PBS for 20 min to reduce nonspecific background staining. Then the samples were washed and for α -actin with Alexa Fluor 488 Phalloidin Conjugate and incubated for 1 h. After that, the samples were dipped in PBS and put on a glassbottomed dish with Vectashield Mounting Medium containing DAPI, which stained nuclei. The images were recorded using a laser scanning confocal microscope.

Fast Fourier Transform (FFT) analysis was used to evaluate the alignment of thin α -actin filaments as a function of the positioning density of PMGI nanofibers.

For this analysis, grayscale 8-bit TIF bright-field microscopic images of α -actin were cropped to 2048x2048 pixels. The resulting FFT output images contained grayscale pixels that represented a frequency and direction. The FFT pattern reflected the degree of α -actin filaments alignment that was present in the original data image.

ImageJ software was used to carry out FFT supported by an Oval Profile plug-in.

The results obtained from the FFT analysis were confirmed by the laser scanning confocal microscopy of stained α -actin filaments. Both the orientation and positioning density of the PMGI nanofibers, influenced the orientation of α -actin in cardiac cells (Fig. 19). While if cardiac cells were cultured on random nanofibers cover slips the α -actin filaments appeared directed in all orientations (**Fig. 26a**).

Cells cultured on cover slips with less amount of nanoimprinted nanofibers displayed a better ordered and elongated α -actin structures as revealed by fluorescent staining (**Fig. 26c**). The α -actin alignment improved with the increase of the positioning density of the nanofibers (**Fig. 26def**). Well-ordered α -actin filaments demonstrated that probably cellular interactions occurring during cell culture growth influenced cell alignment.

α -actin alignment was augmented by a higher density of nanofibers thanks to two process. The first was related to the interactions between the cells and the material, so it attended at the first steps of the seeding. The second one was linked to the cell-cell interactions and it was provided by integrations of the cells. Phase contrast and fluorescent microscopy displayed that PMGI nanofibers imprinted on a solid substrate with a distance less than 30 mm and a density starting from 30 fibers/mm produced an elevate level of anisotropy in cardiac tissue cultures.

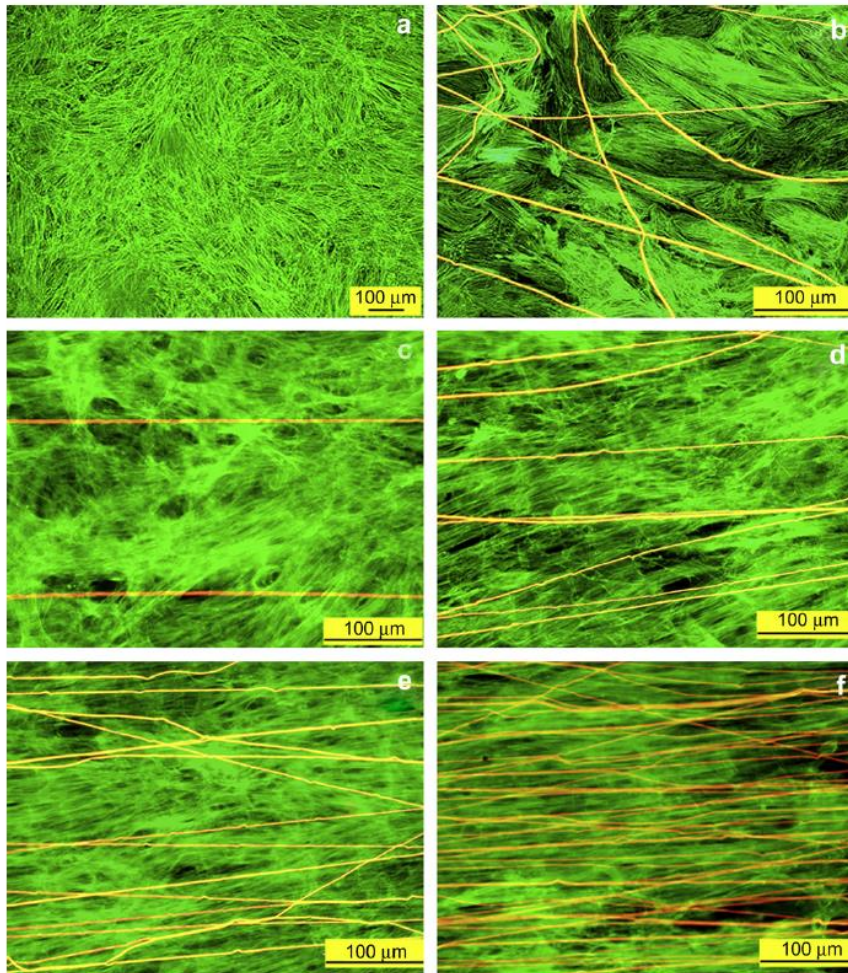


Fig 26. Laser scanning confocal microscopic images of α -actin as a function positioning density of PMGI nanofibers: a culture grown (A) on nanofibers-free solid substrate; (B) on solid substrate covered with randomly distributed PMGI nanofibers; (C-F) on solid substrate covered with aligned PMGI nanofibers at different positioning densities (average distance between the nanofibers): (C) ~ 5 fibers/mm (180 – 150 μm); (D) ~ 10 fibers/mm (120 – 100 μm); (E) ~ 20 fibers/mm (80 – 50 μm); (F) more than 30 fibers/mm (≤ 30 μm) [39].

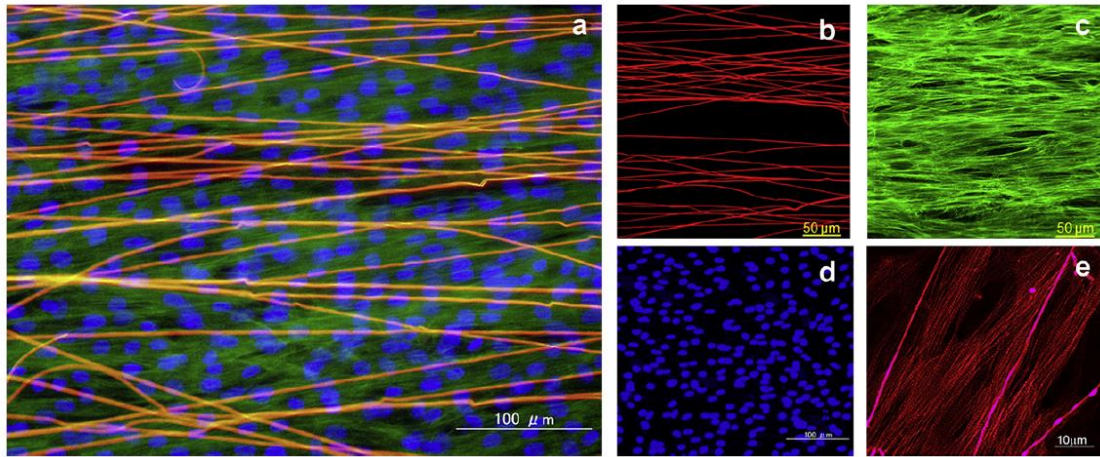


Fig 27. Laser scanning confocal microscopic images of α -actin as a function positioning density of PMGI nanofibers: (A) a culture grown on nanofibers-free solid substrate; (B) on solid substrate covered with randomly distributed PMGI nanofibers; (C-F) on solid substrate covered with aligned PMGI nanofibers at different positioning densities (average distance between the nanofibers): (C) ~ 5 fibers/mm (180 – 150 μm); (D) ~ 10 fibers/mm (120 – 100 μm); (E) ~ 20 fibers/mm (80 – 50 μm); (F) more than 30 fibers/mm (≤ 30 μm) [39].

Fig 27 showed an example of a cardiac tissue culture with anisotropic architecture controlled by PMGI nanofibers. The culture was grown on a solid substrate imprinted with elevate density PMGI nanofibers (~ 50 fibers/mm) with a distance between them of about 20-30 mm (**Fig 27a, b**). This structure showed a high level of cell ordering, α -actin co-alignment along the longer cell axis (**Fig 27c**), parallel arrangement of sarcomeres (**Fig 27e**) and elongated cell nuclei (**Fig 27d**).

2.6) Methods to distinguish cardiac fibroblasts from myofibroblasts

Cardiac fibroblasts have structural, biochemical, mechanical, and electrical conductance roles within the heart. They contribute to cardiac development, myocardial structure, cell signaling and electro-mechanical function in both health and diseased myocardium. They maintain homeostasis of the extracellular matrix keeping balance between the synthesis and degradation of certain factors such as cytokines, growth factors, and matrix metalloproteinases (MMPs). The maintenance of the ECM provides a support for all cardiac cells and acts as an electrical buffer by separating the atria and ventricle to enable proper cardiac function. Fibroblasts secrete also type I and type III collagen. They can repair damaged tissue by migrate and proliferate in the site of injury and producing large amount of collagen.

Cardiac fibroblasts (CFs) contribute to the cardiac electrophysiology. In fact, even if they cannot be electrically stimulated, they provide insulation for myocardial electrical signaling and can generate arrhythmias in disease conditions.

With specific chemical and mechanical stimuli due to fibrosis, such as upregulation of tropomyosin, transgelin, SMemb/nonmuscle myosin heavy chain-B, CFs differentiate in Myofibroblasts, that are large cells with ruffled membranes and contain a highly active endoplasmic reticulum. Myofibroblasts are non-excitabile cells, like fibroblasts and they can impede the electrical conduction bringing to arrhythmias. This cell type activates only after a cardiac injury such as myocardial infarction. Alpha smooth muscle actin (α -SMA) is a fibrous protein highly expressed by myofibroblasts after a myocardial infarction and it is a valid marker of myocardial fibrosis, distinguishing myofibroblast phenotype from cardiac fibroblast one.

The identification of markers able to effectively distinguish myofibroblasts from cardiac fibroblasts remains a great challenge. Aside from α -SMA, Angiotensin 1 receptor (AT 1), transforming growth factor- β type II receptor, paxillin, tensin, and fibronectin extra dominant A are under investigation for this aim. Their expression increased in cardiac myofibroblast cells and may be used in combination with other markers to successfully confirm the myofibroblast phenotype.

In this validation contest, ED-A fibronectin a glycoprotein that can be found in myofibroblast and not in cardiac fibroblast is another promising biomarker. Osteopontin within post-infarcted heart controlled myofibroblasts proliferation and migration. It is expressed both in myofibroblasts and cardiac fibroblasts, however, it is highly expressed in myofibroblasts so it can be a future potential marker to distinguish them.

Tenascin C is a molecule expressed only during pathological conditions especially in the wound-heal process. Tenascin C with other markers, such as desmin, can be used to recognize myofibroblasts type since tenascin C is highly expressed in myofibroblasts but also in other cell lines such as smooth muscle cells [40].

Periostin promotes the recruitment of myofibroblasts increasing collagen production. Shimazaki *et al* [41] showed that in failing heart mRNA expressed Periostin increased. Periostin reappeared after cardiac injury exclusively in myofibroblasts, so Periostin was used as a marker of myofibroblasts.

However, α -SMA in combination with other molecules such as CD45 and CD31 are the most utilized markers to recognize myofibroblasts since they are not expressed by cardiac fibroblasts [40].

Zhao et al [42] created an *in vitro* fibrotic cardiac model by isolating rat cardiac fibroblasts. After they were cultured some of them differentiate in myofibroblasts. Phenotype was assessed by DDR2 (discoidin domain receptor 2) expression (**Fig 28A**), which is a specific marker for cardiac fibroblasts. When the model was set a treatment with a ROCK inhibitor was tested. A high myofibroblasts number was noticed, indicating the potential application of this *in vitro* model for as fibrotic model to test anti-fibrotic drugs.

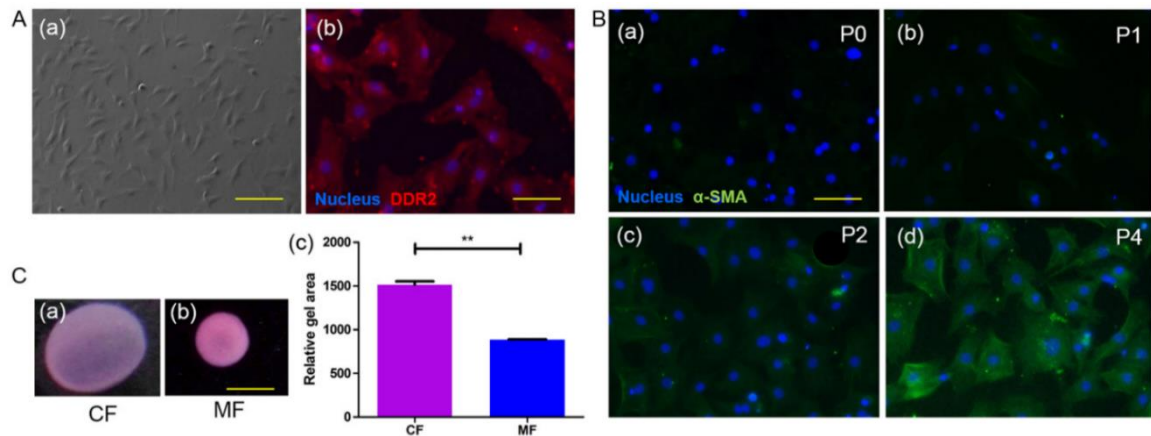


Fig 28. Isolation and characterization of primary rat cardiac fibroblasts. (A) Photo contrast image of freshly isolated rat cardiac fibroblasts (a) and immunostaining of a specific marker for cardiac fibroblasts (DDR2) (b). (B) Expression of α -SMA in cardiac fibroblasts of passages from P0 to P4 (a)-(d). (C) Collagen contraction assay of cardiac fibroblasts (a) and myofibroblasts, (b). Quantitative analysis of gel area was shown in (c). Scale bar. 50 μ m, except for 100 μ m in A (a). [42].

Fig 28B showed that the expression of α -SMA increased during cell passages, and conventional collagen contraction assay displayed that collagen gel produced by myofibroblasts was about half the size of fibroblasts (**Fig 28C**). This was an indication of differentiation of cardiac fibroblasts to myofibroblasts occurred during *in vitro* culture.

Attachment of cells on the substrate was assessed by contrast phase microscopy (data not shown). **Fig 29** displayed the difference in the expression of α -SMA and fibronectin by fibroblasts cultivated on the substrate with the two different rigidity after 1-day culture.

To verify the potential pharmaceutical application of the *in vitro* model a small molecule ROCK inhibitor, Y27632 (a potential anti-fibrotic agent) was used on cells after 1 day of culture and incubated for another 24 h.

The anti-fibrotic potential of Y27632 was revealed by the reducing of phenotypical difference between stiff and soft regions and by the increase myofibroblasts expression profile after the treatment (**Fig 29B**).

By recording the migration profile of cardiac fibroblasts by living imaging and trace tracking was noticed that fibroblasts moved towards infarct region thanks to the mechanical variation between soft and stiff region (**Fig 30**).

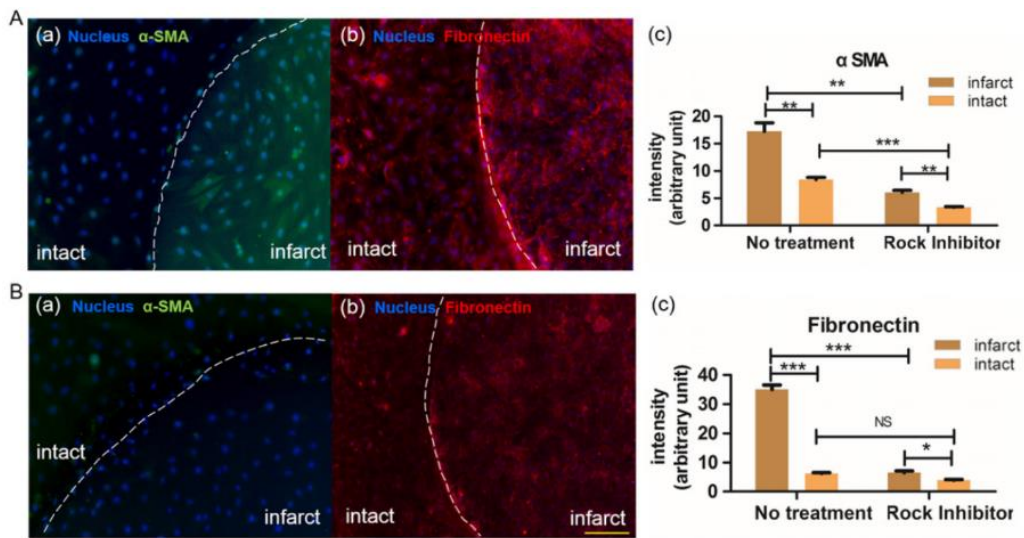


Fig 29. Characterization of the microengineered in vitro cardiac fibrosis model and proof-of-concept demonstration for drug testing. (A) Distinct patterns of α-SMA (a), fibronectin (b) expression were achieved from cells cultured on mechanically patterned substrate. In (c) was displayed the analysis of quantitative comparison. (B) The expression of α-SMA (a) and fibronectin (b) were significantly reduced after the addition of 10 μM Y27632, a commonly used ROCK inhibitor, as shown in (c), while slight difference of biomarker expression between stiff and soft regions might still exist. Scale bars: 200 μm [42].

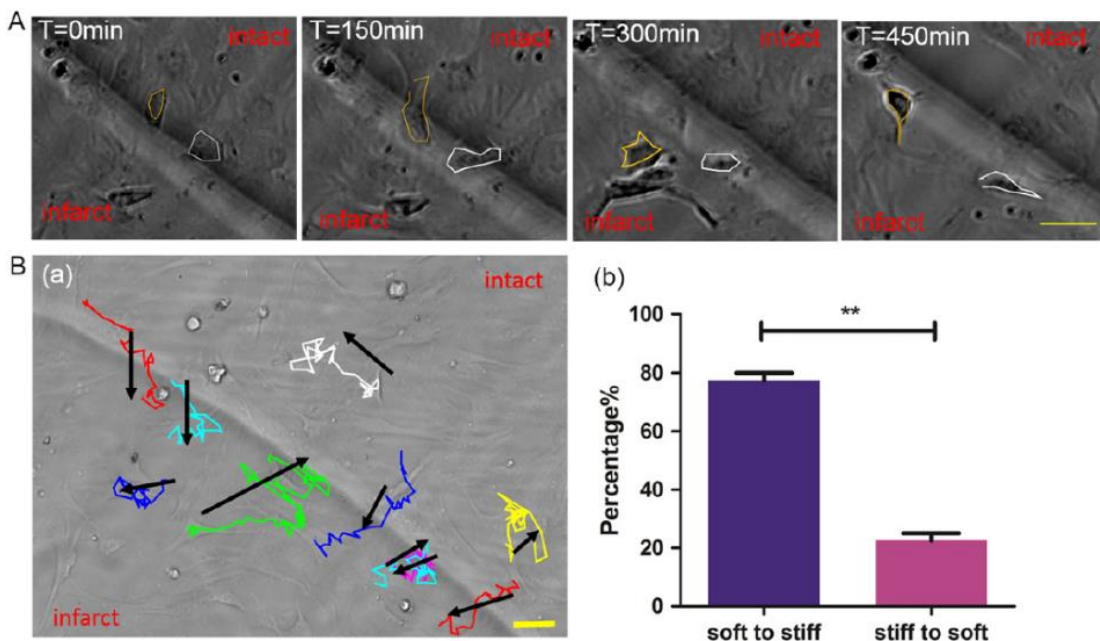


Fig 30. In vitro cardiac fibrosis model reveals that mechanical variation can recruit fibroblasts into the infarcted area. (A) Representative time lapse images showed that cardiac fibroblasts (yellow and white) would migrate across the border from the soft area to the stiff one. (B) Cell movement tracking on the in vitro model. Trace of different cells were identified by specific color lines, with a black arrow showing the direction of cell displacement. The number of cells migrating from to stiff area was quantified and vice versa in (b). Scale bars: 50 μm in A, 20 μm in B [42].

Nagaraju *et al* [43] analyzed the expression of some genes in myofibroblasts (MyoFb) by using reverse transcription quantitative polymerase chain reaction (RT-qPCR). By analyzing the quantity of α -smooth muscle actin [SMA]-positive was seen that MyoFb concentration was greater in heart failure (HF) heart respect to non-HF heart (**Fig 31A**). The expression of fibroblast activation protein alpha (FAP- α), a specific marker of cardiac MyoFb, and of α -SMA (**Fig 31B**), was greater in HF. Colocalization with vimentin or α -SMA staining was assessed around the Ki-67-positive nucleus to show all fibroblastic cells or MyoFb, respectively (**Fig 31C and 31D**).

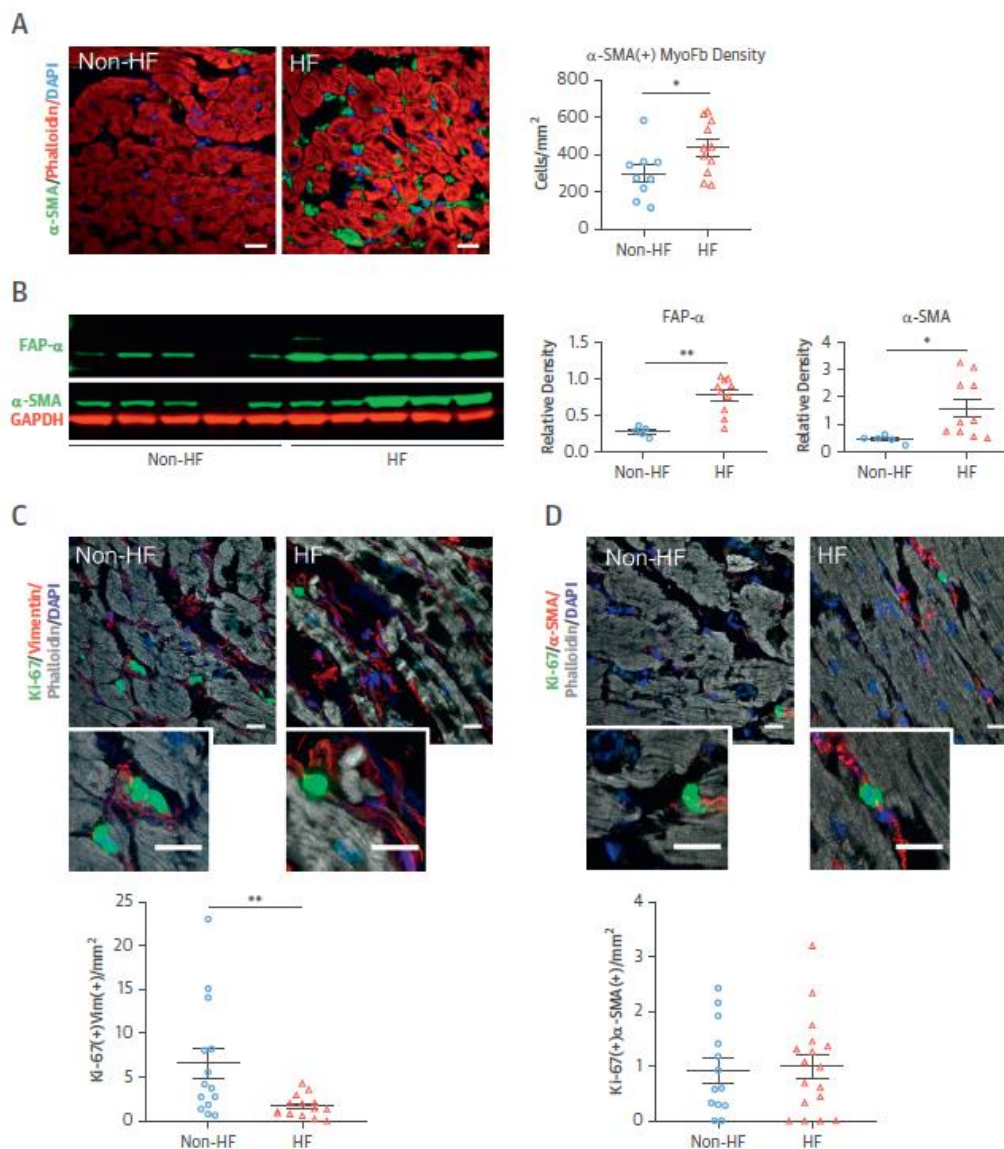


Fig 31. (A) Analysis of density of MyoFb cells based on α -SMA staining $n = 9$ for Non-HF, $n = 11$ for HF. (B) Immunoblot analysis of protein expression for markers of MyoFb, FAP- α (88 kDa), and α -SMA (42 kDa), normalized to GAPDH (37 kDa), in tissue homogenates. $N = 5$ for Non-HF, $n = 10$ for HF. (C) Identification and analysis of cells, both Ki-67 positive and vimentin-positive, representing predominantly fibroblastic cells. (D) Identification and analysis of proliferating α -SMA-positive MyoFb. $n = 14$ for Non-HF, $n = 17$ for HF; for each heart, an area of 4.3 mm² was analyzed. Scale bars represent 20 μ m. * $p < 0.05$, ** $p < 0.01$ (Student t -test, 2-tailed, unpaired) [43].

By using RT-qPCR was revealed that mRNA levels were 8-fold greater than α -SMA (ACTA2) in HF cells (**Fig 32A**).

F-actin stress fibers as a marker for MyoFB differentiation and a double staining for Ki-67 as a nuclear marker for proliferation was used to characterized specific phenotypes (**Fig 32B**). Cells were classified as Fb (ki-67 positive and stress fiber F-actin negative), proliferating MyoFb (p-MyoFb) (Ki-67 positive and stress fiber F-actin positive), and non-proliferating MyoFb (non-p-MyoFb) (Ki-67 negative and stress fiber F-actin positive) (**Fig 32C**) by quantification of phenotype.

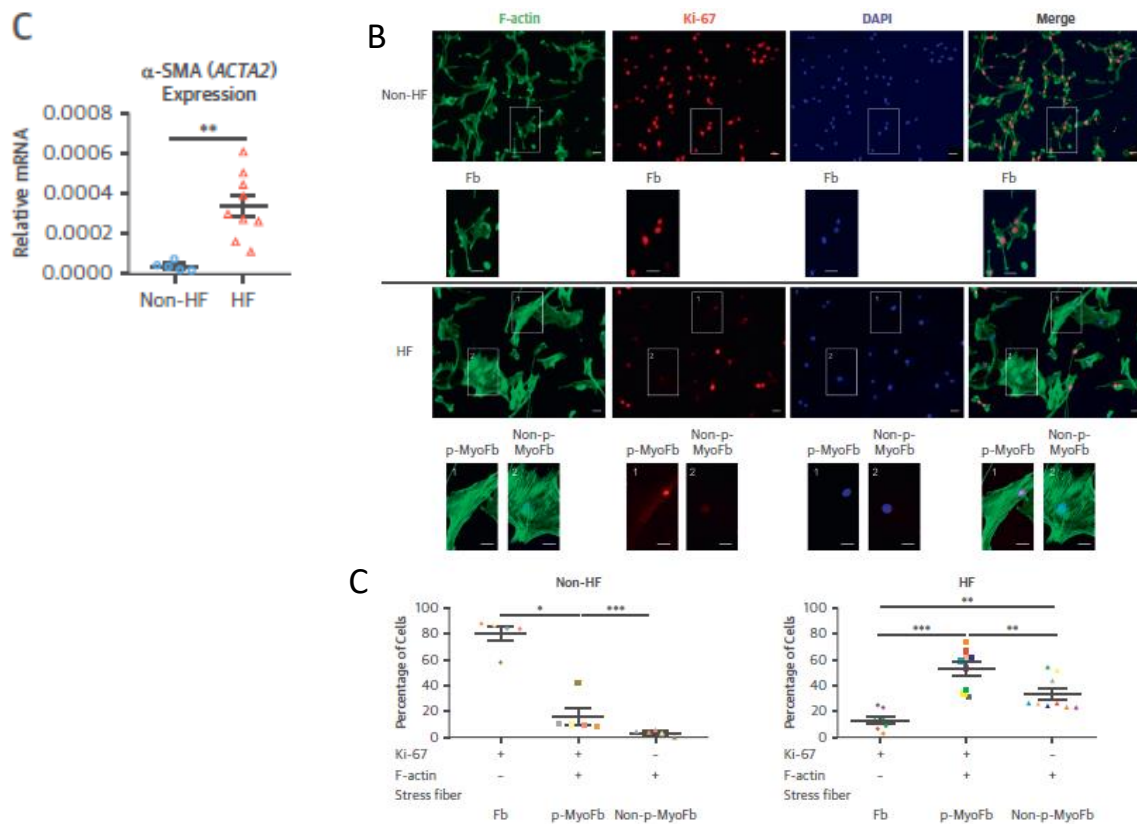


Fig 32. (A) α -SMA (ACTA2) gene expression by RT-qPCR. $n = 5$ for Non-HF, $n = 9$ for HF. (B) Images of immunofluorescent staining of the phenotype marker F-actin (green), the proliferation marker Ki-67 (red), and nucleus DAPI (blue). Scale bars represent $20 \mu\text{m}$. (C) Quantification of phenotype: Fb, proliferating and nonproliferating MyoFb. $n = 5$ for Non-HF, $n = 9$ for HF. Dot colors identify data from the same heart. * $p < 0.05$, ** $p < 0.01$ (Student's t -test, 2-tailed, unpaired for B and C, and 1-way ANOVA with Bonferroni post hoc test for E) [43].

HF MyoFb capacity in matrix remodeling was characterized also by profibrotic genes such as those for monocytes chemo attractant protein (MCP1/CCL2), connective tissue growth factor (CTGF), interleukin (IL)-4, and eotaxin (CC11) (**Fig 32A**), since the expression of them is higher in HF than Non-HF. The expression of these genes was measured by RT-qPCR analysis of mRNA prepared from cell lysates.

For proteins related to turnover of matrix, mRNA expression of MMP3, MMP9 and TIMP1, TIMP2, and TIMP3 was detected in cells isolated from HF hearts (**Fig 32B**).

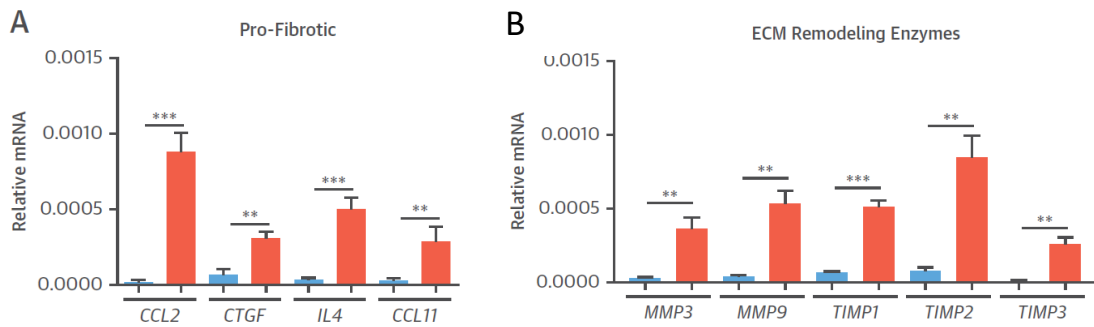


Fig 32. Quantification of gene expression using RT-qPCR after 4-day culture of cells isolated from HF hearts and Noon-HF. (A) Profibrotic genes CCL2, CTGF, IL-4, and CCL11. (B) Genes for the enzymes involved in collagen metabolism: MMP3, MMP9, TIMP1, TIMP2, and TIMP3 [43].

Another interesting marker is miR-29. miRNA is a class of small non-coding single-stranded RNA with a length of about 21-22 nucleotides. It plays a regulatory role by complementary pairing with the 5' or 3' untranslated region (UTR) of the target messenger RNA (mRNA). If the complementary between miRNAs and target mRNAs is high, argonaute-2 in the RNA-induced silencing complex (RISC) causes mRNA to break in the complementary region, leading to gene silencing. Instead, when the degree of complementary is low, miRNA can inhibit the level of translation by regulating the expression of target genes.

Recently, miR-29 was shown to act as a 'master fibro-miRNA' regulator with organ-specific expression. It was also discovered that overexpression of miR-29 in fibroblasts can reduce the expression of fibrosis-related factors, but *in vivo* or *in vitro* inhibition of miR-29 induced expression of fibrosis-related factors. The expression of miR-29 family was reduced near the region of a myocardial infarction in mouse model and humans, and this brought to the release of fibrosis-related cytokines. Besides miR-29 led to the formation of fibrotic tissue in the injured area. The corresponding target of the miR-29 family is the mRNA that encodes the extracellular matrix proteins associated with fibrosis, such as collagen type I, collagen type III, fibrillin-1 (FBN-1), and elastin. It was observed that miR-29 was downregulated after myocardial infarction, which promoted TGF- β from the cell membrane to the cytoplasm, and thus promoting myocardial fibrosis.

Myofibroblasts appear when fibrosis is activated. Since miR-29 is downregulated during fibrosis, it can be used to validate the presence of myofibroblasts. However, this marker

cannot be used alone, but it must be used in combination with other molecules. Besides PCR can be used to evaluate its presence [44].

3) Materials and methods

3.1) Polycaprolactone

Polycaprolactone (PCL) is a FDA approved biodegradable and biocompatible polyester, easily to process through electrospinning, FDM and other biofabrication techniques in tissue engineering applications. It is thermally stable at physiological temperature, in fact, it has a melting point of around 60°C and a glass transition temperature of -60°C. This polymer undergoes hydrolytic degradation of its ester linkages under physiological conditions. In this work, PCL of Mw = 43 KDa supplied by Polisciences was used. This molecular weight it is suitable for FDM process and easy to extrude by compressed air. In **Fig 33** is presented the PCL formula.

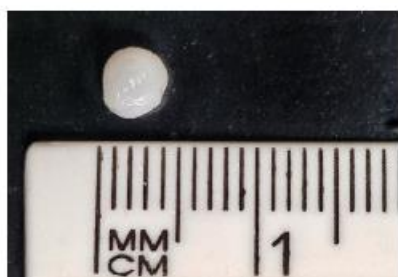


Fig 33. PCL pellets beads

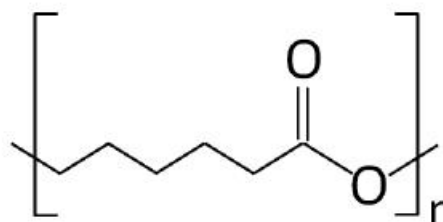


Fig 34. PCL structural formula

3.2) Electrospinning

A 20% wt/v solution of PCL in a Chloroform/Formic Acid mixture (70/30 v/v) was prepared (Chloroform 99.8% and Formic Acid 98% were purchased by Sigma-Aldrich). Chloroform has a high evaporation rate and this quality is very suitable for this technique. The solution was stirred for about 2 hours after dissolving PCL pellets (**Fig 34**) in Chloroform. The addition of Formic Acid is required to enhance the polymeric solution conductivity. Formic Acid increases the spinnability of the solution since it has a high polarity. Moreover, this strong polar acid allows the deposition of fibers with a reduced diameter. Then, the prepared solution was stirred for about 40 minutes at 200 rpm to permit complete Formic Acid dispersion.

Electrospinning setup (**Fig 35**) for random and aligned fibers collection includes:

- 1) A 200 mm x 300 mm flat collector covered with two aluminum sheets for random fibers deposition;
- 2) A rotating spindle covered with two aluminum sheets for aligned fibers deposition;
- 3) A 5 mL syringe containing the polymer solution to be extruded with a 21 G needle;
- 4) A pump that applies a continue pressure to extrude the solution from the syringe;
- 5) A high voltage generator that contains the interface to set the process parameters for the voltage generation and the rotation of the spindle.

For the collection of random fibers, the flat collector was grounded connected through a clamp, while syringe needle was connected to the positive output of generator.



Fig 35. Electrospinning setup

For the collection of the aligned fibers the extremities of the rotating spindle were grounded connected, while the positive output was connected to the syringe.

3.2.1) Process optimization

A previous optimized protocol for the collection of PCL random fibers was used as starting point to further optimize the process of nanofibers membranes production [45].

The parameters of the previous protocol are summarized in **Tab 2**:

Solution Parameters	Process parameters
Polymer concentration = 20%w/v	Voltage = 15 kV
Primary solvent concentration = 70%w/v	Flow rate = 0.5 mL/h
Secondary solvent concentration = 30%w/v	Distance tip_collector = 15 cm

Tab 2. Previous protocol parameters

A flow rate of 0.25 mL/h was set to increase the time that the fibers take to reach the collector and to allow a slow solvent evaporation. Needle-collector distance was reduced to 12 cm. On the other hand, for aligned fibrous membranes we set the same process and solution parameters. 2000, 2500 and 3000 rpm rotation speed of the spindle were tested. All the electrospinning experiments were carried out at room temperature and room humidity.

3.2.2) Membranes fabrication

The parameters of the optimized protocol for random fibers are synthesized in **Tab 3**.

Solution Parameters	Process Parameters
Polymer concentration = 20 %w/v	Voltage = 15 KV
Primary solvent concentration = 70 %w/v	Flow rate = 0.25 mL/h
Secondary solvent concentration = 30 %w/v	Distance tip-collector = 12.5 cm

Tab 3. Optimized protocol parameters of random fibers

The parameters for the fabrication of membrane with aligned fibers are listed in **Tab 4**.

Solution Parameters	Process Parameters
Polymer concentration = 20 %w/v	Voltage = 15 kV
Primary solvent concentration = 70%w/v	Flow rate = 0.25 mL/h
Secondary solvent concentration = 30%w/v	Distance tip-collector = 12cm
	Rotating speed = 3000 rpm

Tab 4. Optimized protocol parameters of random fibers

To get the samples for the *in vivo* culture of fibroblast some special coverslip glasses were stuck on the last aluminum foil, with conductive tape.

3.4) Functionalization process

3.4.1) Polydopa-gelatin functionalization

PCL is an hydrophobic material, so it has low affinity with cells. To improve its hydrophilicity, 2D scaffolds were coated with 3,4-Dihydroxy-DL-phenylalanine (DOPA, Sigma Aldrich-Milano) and porcine Type A Gelatin (Sigma Aldrich-Milano). The polymerized form of the DOPA is widely used as adhesive molecule. DOPA polymerize in mild basic conditions sticking on the exposed surface of the scaffold. This protein has a high affinity with a wide range of substances, and it can better link the scaffold to the functionalizing protein. For the functionalization process was used as basic buffer a solution of tris (Tris(hydroxymethyl)aminomethane) (Sigma Aldrich – Milano) dissolved in bi-distilled water, to which was added HCl solution (1 M) to reach pH = 8.5.

The first functionalization step was the attachment of polyDOPA to scaffold. DOPA was dissolved in the basic buffer solution with a concentration of 2mg/mL. When the solution started to take a brownish color, the scaffolds were immersed. They were left there for 7 hours. After this time the scaffolds were took out and washed with the buffer solution by soaking for 5 min for three times.

The second step involved the functionalization with Gelatin. Gelatin was dissolved on the buffer solution with a concentration of 2mg/mL and the solution was put in stirring at 100 rpm and at 40°C for 1 h. When the Gelatin was completely dissolved, this solution was left to cool down until room temperature. Next, scaffolds were immersed in this solution for 16 h on static conditions. Later, they were washed in buffer solution three times as previously described and then in bi-distilled water. Then the samples were dried under hood and later put in the fridge to preserve gelatin coating integrity.

3.5) PCL Scaffolds characterizations

3.5.1) Scanning Electron Microscope (SEM)

Electrospun scaffolds morphology was evaluate through SEM analysis also to identify eventual surface defects. In this way the process could be optimized if necessary. Samples were previously coated with a gold layer by using Agar Auto Sputter Coater instrument setting the following parameters: execution time equal to 50 s and current equal to 39 mA. After that, the samples were placed in the chamber of the SEM LEO 435VP SEM to be analyzed.

SEM images with 1000x, 2000x and 5000x magnifications were obtained.

3.5.2) ImageJ Software

SEM images were processed with ImageJ digital image processing software (National Institute of Health, USA). This software was used to obtain the numerical data to graph the distribution of diameters and porosity of the electrospun membranes. The distribution was obtained by taking 50 measures of the diameter fibers on SEM images with higher magnification (5000X). While for the qualitative analysis of porosities was set the threshold parameters arbitrarily. Excel software was used to process the data, to calculate average diameter and standard deviation.

3.5.3) Contact angle

This technique was used to evaluate the hydrophily of the surfaces of the scaffolds. The success of a functionalization process can be studied through this technique. Besides, contact angle instrument (**Fig 37**) can evaluate which of the functionalization is more effective to increase the wettability of the surface. The sample was put on a glass slide and placed on the contact angle support. The support moved through three wheels in the three direction X-Y-Z. The sample was put between a blue light source and a camera. Images were taken by the camera that send data to a computer that elaborate them. PC showed on the display the taken images superimposed with lines that showed the shape of the drop, baseline, direction of the

liquid-air interfacial energy and the angle between liquid-air interface and the baseline. Above the plate there was the syringe that made and release the droplet on the sample. The interface of the software allowed to select the time in which the operator wanted to start the image frames acquisition and the time in which the acquisition must stop, with a range of 10 s maximum. During this process the operator could decide to adjust the baseline manually or automatically. After that, software calculated the contact angle for each acquired photogram.

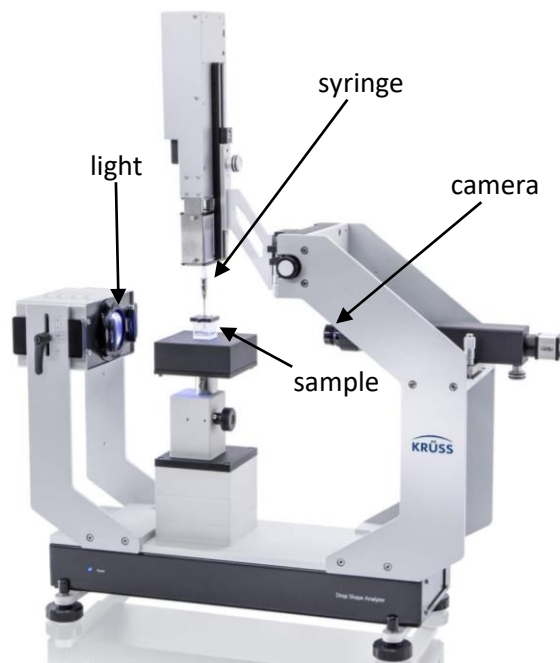


Fig 37. Contact angle set up instrument

3.5.4) Solvent casting

PCL films was prepared via solvent casting (**Fig 38**) to characterize each functionalization step without taking in account the morphology of both 2D and 3D scaffolds. The process consisted of three main steps. Firstly 5 g of PCL pellets was dissolved in 50 mL of Chloroform (Sigma Aldrich – Milano) in order to have a 10% w/v PCL solution. The obtained solution was placed into a 11 mm diameter glass Petri disk placed under hood, covered with a perforated aluminum foil and then with a 2L Becker, in order to decrease chloroform evaporation rate and to produce a more homogeneous PCL sheet. PCL were then functionalized with the same procedures used for scaffolds obtained by Electrospinning and FDM.

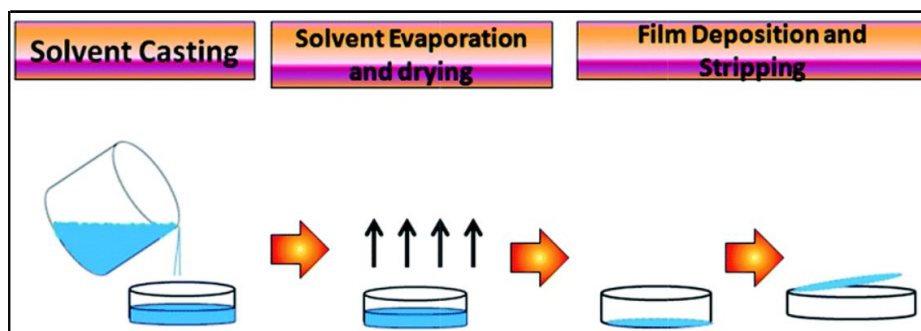


Fig 38. Solvent casting process steps: 1) PCL/Chloroform solution prepared and poured out into petri dish, 2) solution is dried 3) PCL film is removed.

3.5.5) Acid Orange UV-Vis

Acid Orange (AO) colorimetric assay was carried out to evaluate the stability of surface amino group in three-time steps: 1, 3 and 7 days. Four samples per time steps were produced, one for each kind of functionalization, DOPA, gelatin, DOPA/gelatin and non-functionalized. Then the samples were left in PBS for the required time. AO solution was produced dissolving 0.175 mg/mL of Acid Orange (II) (Sigma Aldrich- Milano) in pH 3 water solution. Samples were dipped in AO solution overnight at room temperature. Samples were then immersed in 4 mL of pH 12 water solution for 30 minutes at room temperature in order to release the AO molecules from the sample surface. The obtained eluate was analyzed using Biotek plate reader at 485 nm. Calibration curve, reported in **Fig 39**, was obtained by analyzing several AO solutions at pH 12 with known concentration. The concentration of amino groups was obtained using the calibration curve. Then the number of moles/cm² was gotten with formula 1 and formula 2.

$$\text{Amino group weight density} = \frac{\text{Concentration} * \text{volume of the plate reader section}}{\text{sample surface}}$$

Formula 1

$$\text{Amino group moles density} = \text{Amino group weight density} * \frac{\text{number of moles}}{\mu\text{g}}$$

Formula 2

The number of moles/μg refers to amino groups. But formula 2 can be used because a molecule of acid orange link to one amino group. The number of moles/ μg for the acid orange is a value on the package.

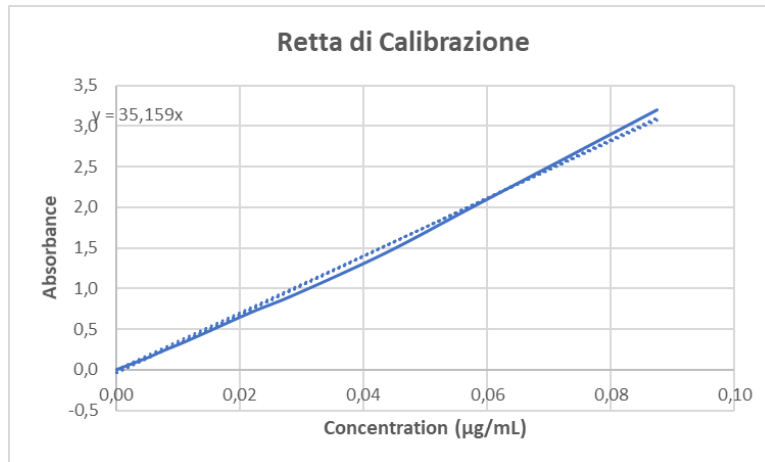


Fig 39 Calibration curve for AO analysis

3.5.6) Degradation Analysis

Degradation analysis was conducted to evaluate the degradation rate of the electrospun mats in a like *in vivo* environment. The experiment was carried out for 1, 3, 7, 14, 21 and 28 days. For each time step, four samples with a weight between 14 and 18 g were used. To emulate the *in vivo* conditions, the samples were dipped in PBS solution and they were incubated in a hove at 40°C and the solution was refreshed every 3 days. The dried sample were weighed before and after the incubation. The degradation trend for each time steps were represented by a histogram, where the average percentage variation weight respect to the initial weight of the samples is displayed. The histogram is a function of the time steps.

4) Results

4.1) Scaffold fabrication

4.1.1) Scanning Electron Microscopy (SEM)

Electrospun membranes morphology was assessed by Scanning Electron Microscopy (SEM). Fig1 and Fig2 refer to different parameters sets to build up random and aligned fibers.

4.1.1.1) Random fibers

Fig 40 displayed the two steps of optimization protocol, the effect of the distance between the collector and the needle was evaluated.

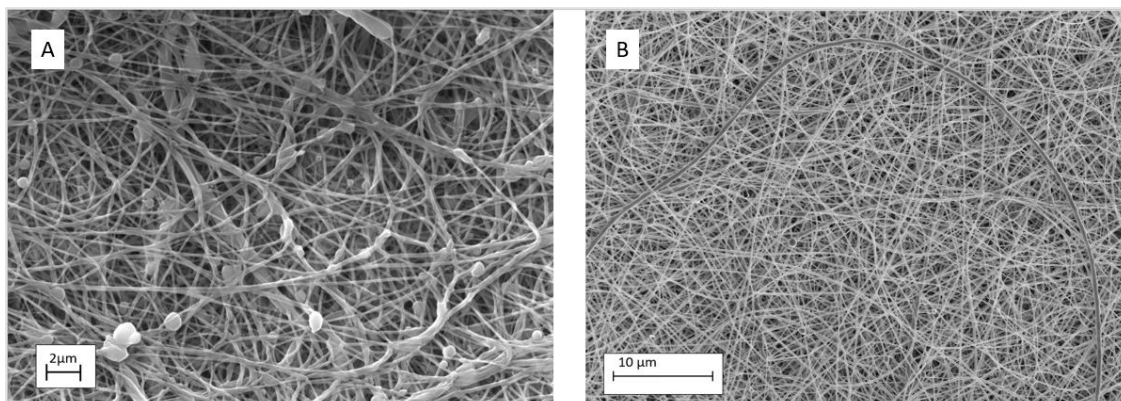


Fig 40 SEM images of the PCL43 random fiber membranes. A) Fibers obtained from the previous protocol ($D=15\text{cm}$) with a magnitude of 5000X. B) Fibers obtained from the new protocol ($D=12\text{ cm}$) with a 5000X magnitude.

Fig 40A showed random fibers obtained with a previous set of process parameters (30/70 chloroform/formic acid, 20% w/v of PCL, 15 kV, 15 cm, 0,5 mL/h). The collected fibers presented a not uniform morphology with a lot of beads and ribbons. These defects were probably due to the incomplete evaporation of solvent before reaching the collector. Besides, under these working conditions, electrospinning process resulted very instable and the continuous drip near the tip prevented polymeric jet formation. So, the flow rate was reduced from 0.5 mL/h to 0.25 mL/h. Then the distance between collector and needle was increased to permit a complete evaporation of the solvent but the jet remained unstable since

drops formed at the tip of the needle. So the distance from the collector was reduced to 12 cm.

Tests have shown that flow rate was the most influential parameter. Firstly, applied voltage was increased to further charge the solution.

But in this case some macroscopic hillocks formed on the surface of the membrane by increasing the voltage above 15 kV. So, the voltage was left to 15 kV.

Once the protocol was optimized (30/70 chloroform/formic acid, 20% w/v of PCL, 15 kV, 12 cm, 0,25 mL/h) membrane were made through a continuous electrospinning process of 6 h. Membrane created had more uniform morphology and fibers dimensions, there wasn't defects and macro defects were absent.

The image b) of Fig 40 displayed the results obtained with the new protocol.

4.1.1.2) Aligned fibers

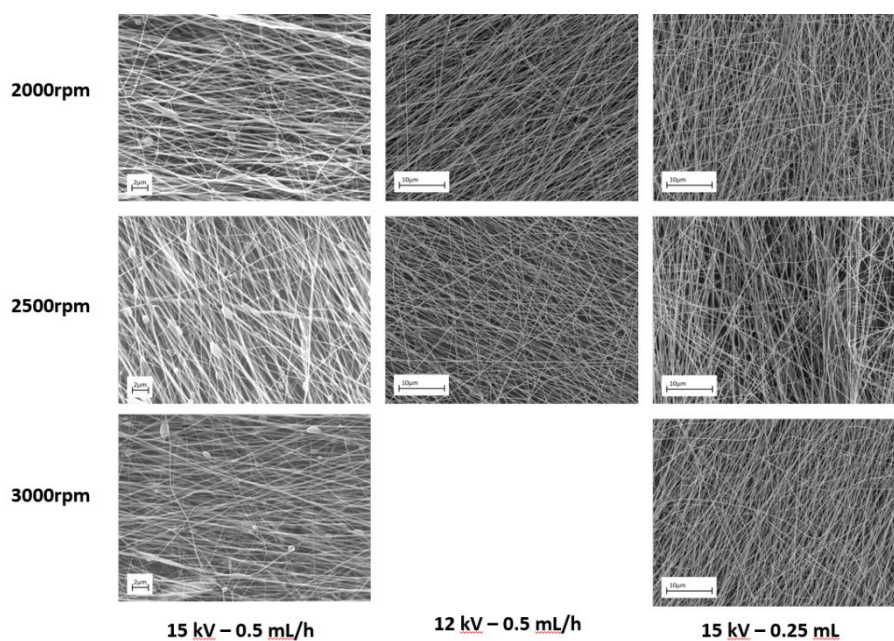


Fig 41 SEM images of PCL43 fibers in the three steps of the process optimization with the purpose to establish the best parameters to obtain aligned fibers with the minor amount of defects.

Fig 41 showed the effect of applied voltage, flow rate and spindle rotating speed on fibers morphology and alignment grade. With high voltage and high flow rate the solvent did not have time to completely evaporate, so there were a lot of defects on the membranes. By testing the changing the voltage reduction and flow rate separately on defects and alignment level has been noticed that the defects decreased with the reduction of one of the parameters

between applied voltage and the flow rate. The distance from the collector could influenced the morphology of the fibers but our setup impeded to increase this parameter since the distance was already at the maximum. Both modifications led reduced defects, however voltage decrease conducted to the deposition of more homogeneous fibers. Besides the figure showed that with a speed of rotation of 2000 rpm the fibers are already aligned, even if 3000 rpm gave slimmer fibers, besides the analysis of the alignment made with imageJ showed that the peaks were more pronounced with this speed (**Fig 42**).

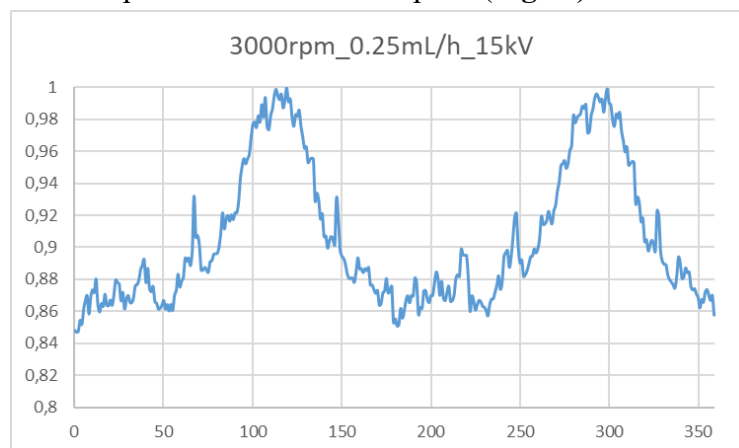


Fig 42. FFT on SEM image of a membrane obtained with the optimized set of parameters (3000rpm, 0.25 mL/h, 15 kV).

4.1.2) ImageJ software

Fig 43 showed the percentage distributions of nanofibers diameter for each set of parameters tested during the optimization of aligned fibers protocol. The best results were obtained with 3000 rpm, since lower average diameter and standard deviation were gotten with it.

In fact, the average diameter is 217 nm and the standard deviation is 34 nm. While for the other sets of parameters the values of standard deviation was above 50 nm or a little bit less. It was noticed that diameters decreased with the increase of rotation speed. As the rotation speed increased, the traction mechanical stress to which the fibers were subject increased, making them thinner. Another parameter that influenced the fiber diameter was the applied voltage. When the voltage was higher the diameter was lower as such as for the random fibers.

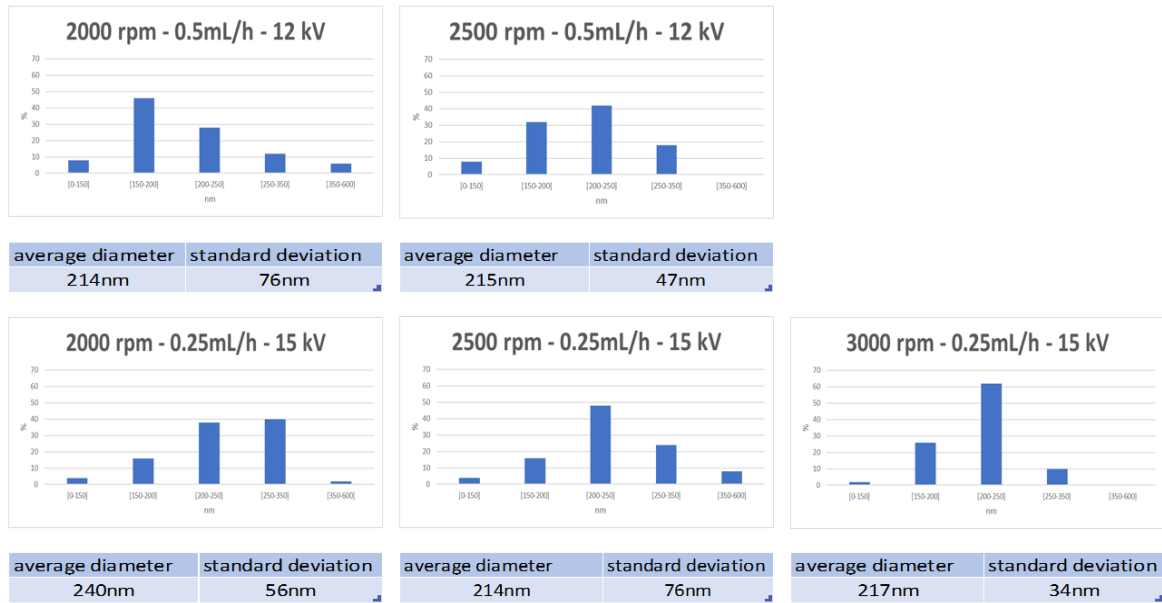


Fig 43. Analysis of dispersity of the diameters in the aligned fibers for the various set of parameters.

When the velocity of the spindle was 3000 rpm only some percentage fell out of 150 nm. The analysis of the porosity was carried out by analyzing with imageJ the SEM image of the membrane. To make this analysis each porosity was consider circular and planar. After the area was calculated the diameter of each was got in Excel (**Fig 44**). Most diameters were in the range of 0.3-0.5 μm .

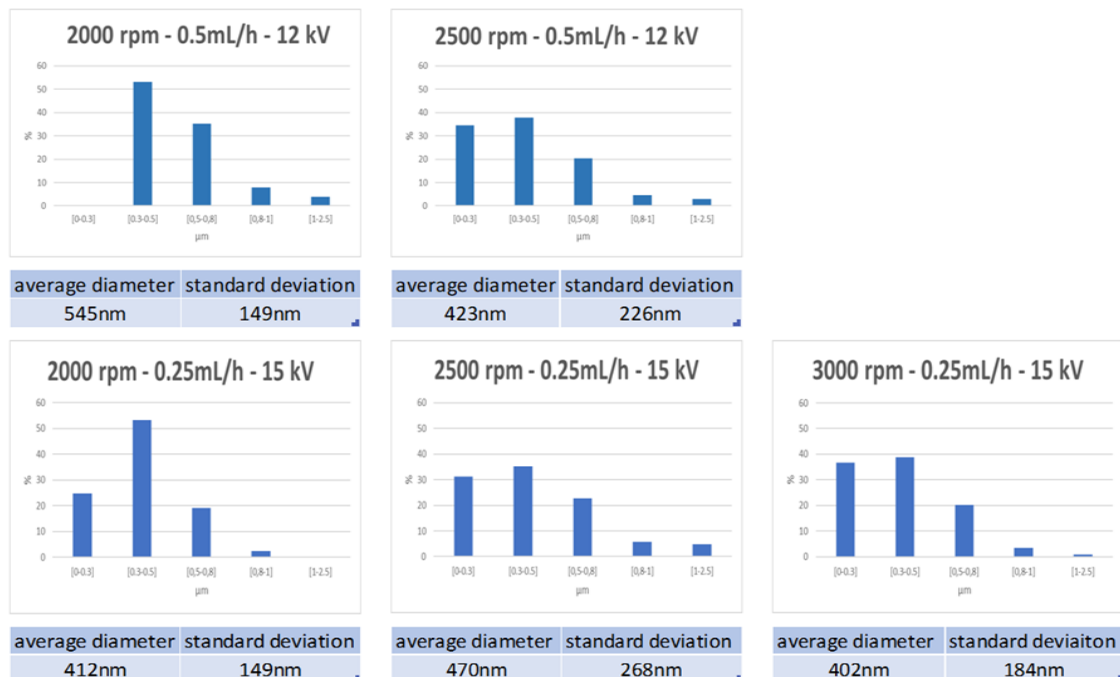


Fig 44. Porosity analysis in the aligned fibers for the various set of parameters.

4.1.3) Degradation Analysis

This analysis was carried out to evaluate the stability in physiologic environment of the electrospun membranes up to 4 weeks. The loss of material during this period was very low. In the first weeks significant changes in weight were not appreciate, the minimum loss in the fourth week could be due to scarce precision of the instrument (1mg) compare to the weights presented (**Fig 45**).

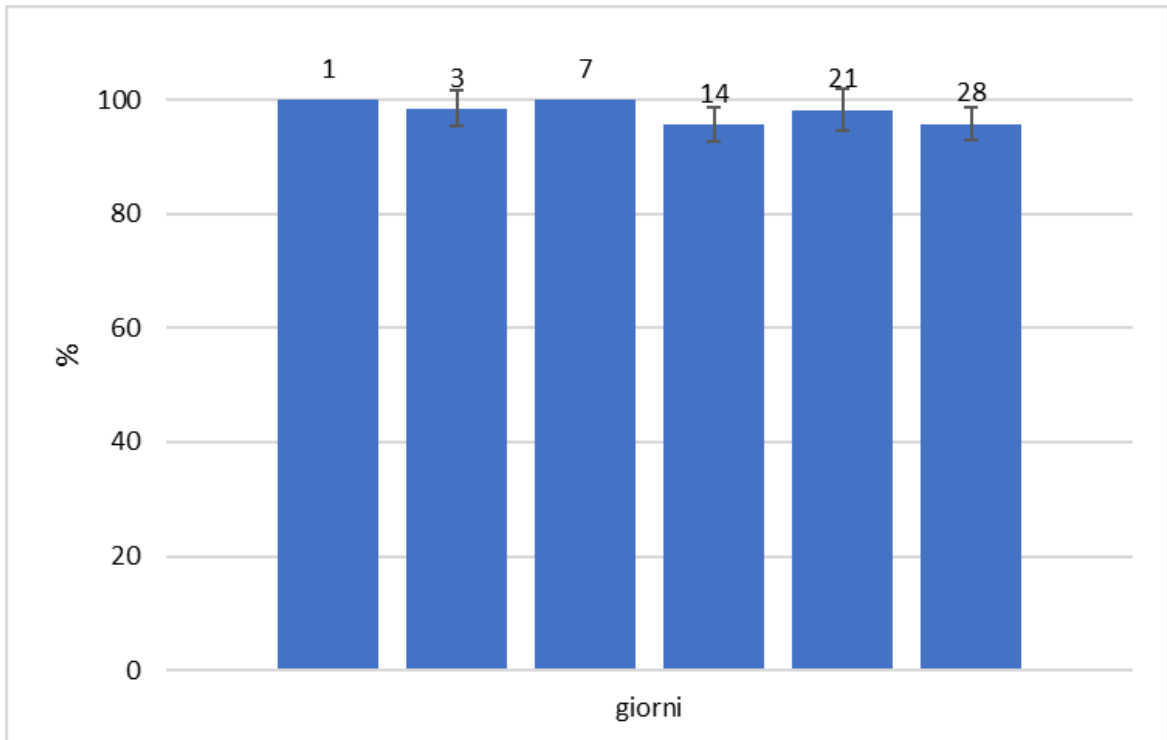


Fig 45 Percentage of weight left after the corresponding time step.

The maximum leak of weight corresponds to 4.25% that is a very modest value, in fact, PCL takes about 6 months to degrade completely in *in vivo* condition.

In the **Fig 46** SEM images of a PCL membrane is displayed. Even if the time of incubation in PBS was low respect to the time of degradation of the PCL in *in vivo* condition some signs of degradation started to compare especially with the longer time steps as 21 and 28 days.

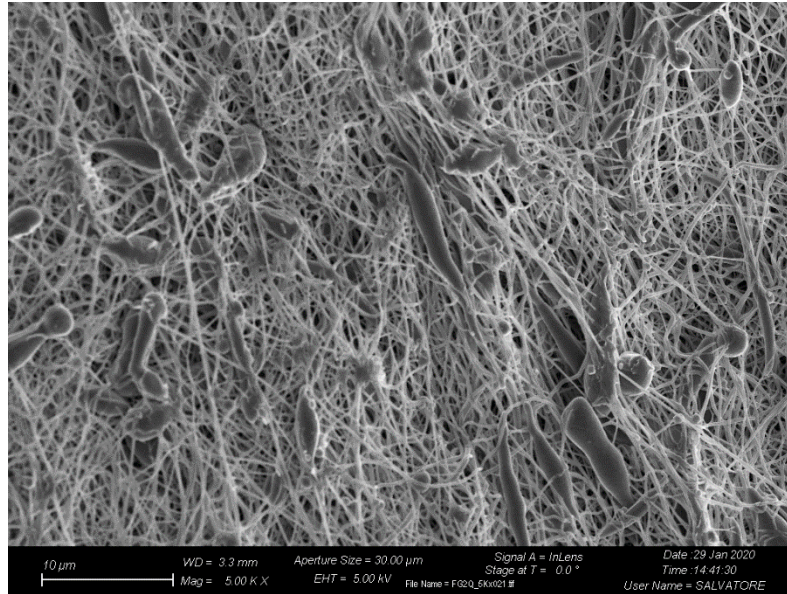


Fig 46 SEM images of random fiber membrane degradation after 28 days of incubation in PBS solution.

4.2) Scaffold functionalization

4.2.1) Contact angle

The measure of the contact angle on the scaffold with different functionalization was used to assess the hydrophilic characteristic of the surfaces.

Six measures were done for each material. Three measures for each contact angle at the time $0s(t_0)$ and $5s(t_5)$ was taken, where the zero time was the time in which the drop contacted the surface. The analysis was carried out on solvent casting membrane. **Fig 47** and **Tab 5** showed that the non-functionalized membrane was the more hydrophobic material with an angle at t_5 of 141.08° . With the functionalization in DOPA the material started to become more hydrophilic, but the best results were obtained with the functionalization with DOPA/gelatin since it had a contact angle of 62.03° at t_5 . The functionalization in Gelatin gave better results than the one with DOPA because the layer in Gelatin was more hydrophilic. While the functionalization in DOPA/gel had a contact angle lower than Gelatin because the layer of DOPA made possible to attach a major quantity of Gelatin and this is reflected on the contact angle at t_5 . So, the functionalization in DOPA made the functionalization more stable and homogenous.

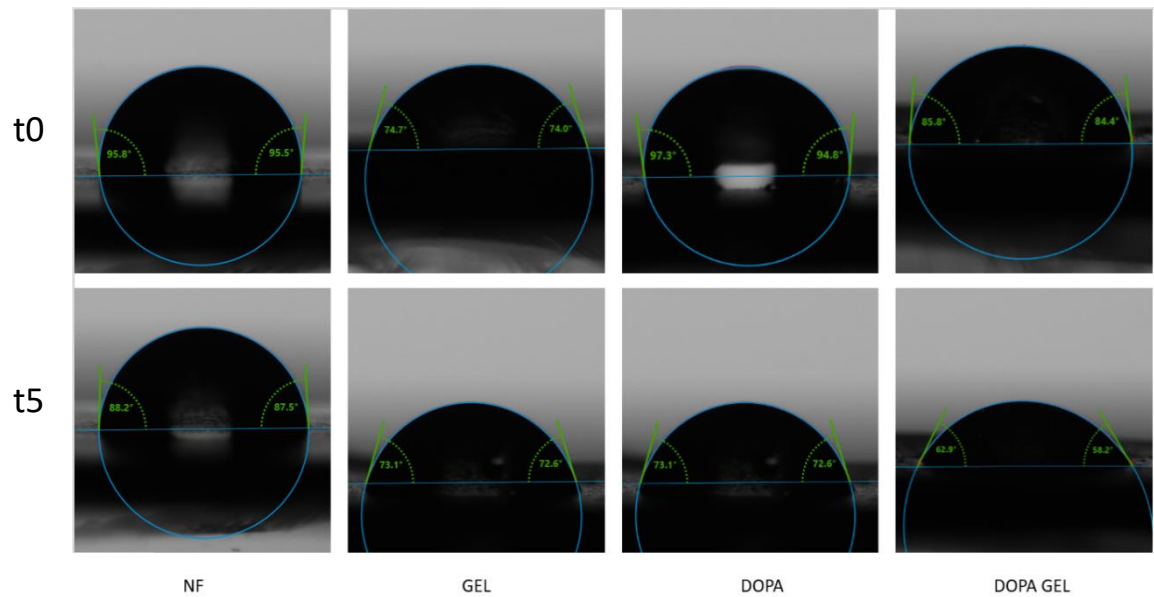


Fig 47 Contact angles on the 4 kind of surfaces analyzed at the two different time steps

Colonna1	NF	GEL	DOPA	DOPA GEL
t0	140.08	80.27	93.07	96.55
t5	141.08	64.70	74.62	62.03

Tab 5 Average of the three measures made for the right and left contact angles for the 4 kind of surfaces.

4.2.1) Acid Orange UV-Vis

This analysis gave feedback about how many surface amino groups are presented on the scaffold. These groups typically come from gelatin, so more acid orange settles, more amino group were on the surface and more gelatin was on the samples.

Fig 48 showed the average of the concentration of amino groups in all the four samples. The concentration on the PCL-polyDOPA/Gel was higher than the other three substrates in fact, it had 0.0043 n moles/cm² at the first day. This result was in line with the expectation since the DOPA layer should increase the stability of the gelatin layer. The presence of a quantity of acid orange even if in the sample non functionalized and functionalized with only dopamine was probably due to a partially absorption of the acid orange on the sample. While for the samples with dopamine the presence of acid orange was probably due to the presence of an amine group in the structure of the molecule. Even though the presence of the amino groups was greater in collagen molecule.

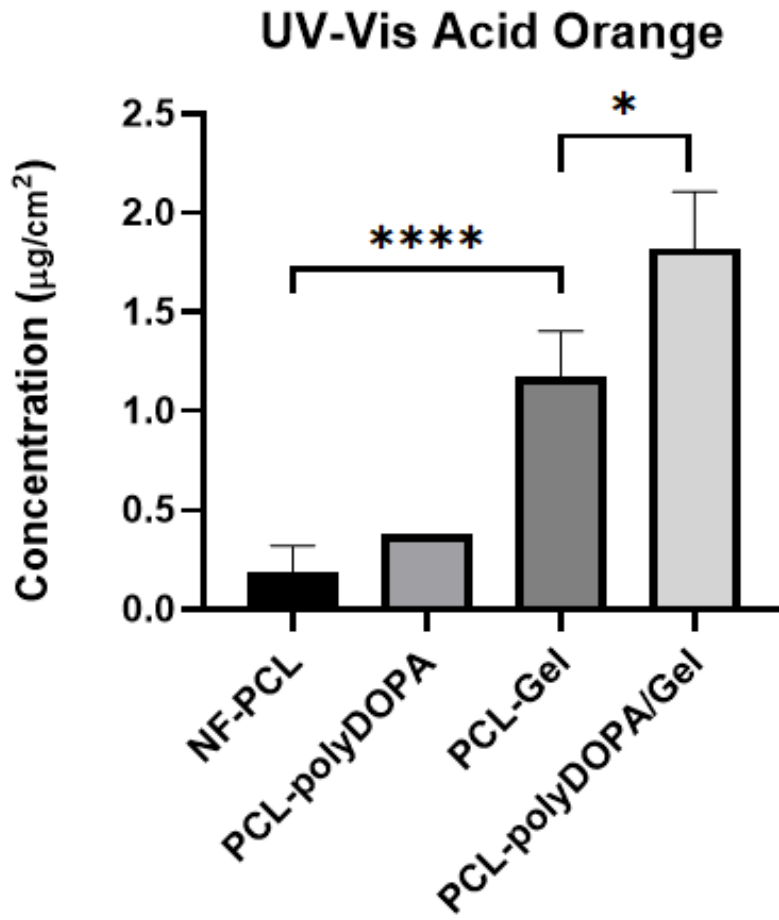


Fig 48. Average of concentration of amino groups detected with acid orange assay.

In **Tab 6** was displayed the trend of the concentration of the four samples in at 7 days. The layer with DOPA make the gelatin layer more stabilized also after 7 days.

These results showed the correct functionalization of the scaffold both with gelatin and dopamine and gelatin together.

1 d	Sample	Absorbance	Concentration (ug/mL)	ug/cm ²	n moli/cm ²
	PCL_NF	0.0027	0.0792	0.1583	0.0006
	PCL-poliDOPA	0.0080	0.2375	0.4750	0.0019
	PCL-Gel	0.0067	0.1979	0.3958	0.0016
	PCL-poliDOPA/Gel	0.0183	0.5443	1.0885	0.0043
3 d	Sample	Absorbance	Concentration (ug/mL)	ug/cm ²	n moli/cm ²
	PCL_NF	0.0077	0.2276	0.4552	0.0018
	PCL-poliDOPA	0.0083	0.2474	0.4948	0.0020
	PCL-Gel	0.0120	0.3563	0.7125	0.0028
	PCL-poliDOPA/Gel	0.0140	0.4156	0.8313	0.0033
7 d	Sample	Absorbance	Concentration (ug/mL)	ug/cm ²	n moli/cm ²
	PCL_NF	0.0063	0.1880	0.3760	0.0015
	PCL-poliDOPA	0.0120	0.3563	0.7125	0.0028
	PCL-Gel	0.0067	0.1979	0.3958	0.0016
	PCL-poliDOPA/Gel	0.0193	0.5740	1.1479	0.0046

Tab 6. Concentration of amino groups linked on the surface of the four kind of scaffolds for the three different time steps. In the first column there is the absorbance detected by the instrument, in the second the concentration calculated by using the calibration curve, in the third the concentration respect to the surface of the sample (1mm) and in the last the number of moles respect to the surface.

5) Conclusions

The process for approving a new drug is very complex. This is due to experimental tests on animals and humans that this new drug must overcome before being placed on the market. However, the animal model is not so predictive about the drug effects and toxicity on human organism. Increasing interest is directed towards *in vitro* models capable of replicating the tissue under examination with high reliability. *In vitro* models represent a valid platform for disease modelling and preclinical drug screening. The organ on which drugs often cause problems is heart, which is why many efforts have been made to try to develop satisfactory models for cardiac tissue applications.

However, it is often needed to reproduce the pathological condition of a specific tissue or organ, since drugs must be tested on pathological subjects and organs that could react differently from healthy tissue. In literature a lot of works on *in vitro* models have the purpose to be used for regenerative tissue engineering rather than the creation of pathological models to test new drugs. Moreover, *in vitro* models are used to differentiate cells by using physic-chemical characteristics of the scaffold. In addition, in their physiological environment, cells need a lot of stimuli such as growth factors, hormones and chemical signals coming from surrounding cells or either from the blood flow, so from more distant cells. So a step forward for the construction of models would be to incorporate these stimuli in the culture medium.

About the work done in this thesis, to produce the electrospun scaffold, we started from a previous protocol. SEM images showed a lot of morphological defects, so an optimization of process parameters was carried out. In order to favour a good evaporation of solvents, avoiding the collection of beaded fibres, we reduced the flow rate (0.25 mL/h). Besides, to avoid solution dripping we decided to slightly reduce the distance between tip and grounded collector (12 cm).

In the future developments aligned electrospun scaffolds can be used for human cardiac fibroblasts seeding obtaining a versatile *in vitro* cardiac fibrotic model that emulate the various stages of fibrosis. Then the model can be validated with the techniques found on literature. The first type of characterization is the evaluation of the shape and orientation of the cells by using staining.

Hussain et al exploited immunochemistry to assess the expression of SM-actin and the expression of gap junction protein Cx43 in the system. For this kind of characterization samples were dipped in PBS and then permeabilized in Triton X with PBS. Next primary

antibody was added and incubated and with secondary antibody. At the end the samples were analyzed with fluorescent microscopy.

Another strategy was the PCR, that allowed to evaluate the gene expression of the cells under culture. Brown et al used RNeasy to isolate total RNA by lysing cells, then QiaShredder columns were used to homogenize. UV light was used to determine RNA concentration in the sample. TAMRA at the 3' end and FAM, VIC and TET at the 5' end were utilized to modified fluorescent TaqMan probes for glyceraldehyde-3-phosphate dehydrogenase (GAPDH), ANF, and β -MHC, respectively.

Then methods were searched to distinguish myofibroblasts from cardiac fibroblasts. Tarbit et al [42] found that aside α -SMA other markers can be used for this purpose. There is Angiotensin 1 receptor (AT 1), transforming growth factor- β type II receptor, paxillin, tensin, and fibronectin extra dominant, since their expression increases in myofibroblasts.

Shimazaki et al [43] showed that in failing heart mRNA the expression of Periostin is higher. Periostin appear only in myofibroblasts so it is a good marker of this type of cell.

In addition, the use of miRNA-29 is a good strategy to distinguish myofibroblasts from cardiac fibroblasts. miRNA is a small non-coding single-stranded RNA that plays a regulatory role and inhibit the level of translation by regulating the expression of target gene. The activation of cardiac fibroblasts is observed also by analyzing miRNA level, since the differentiation in myofibroblasts is also caused by a downregulation of miRNA levels, that regulate cardiac fibroblasts behavior and caused their activation.

Bibliography

- [1] Hou, Z., Xue, C., Peng, Y., Katan, T., Kistler, H. C., & Xu, J. (2002). A Mitogen-Activated Protein Kinase Gene (MGV1) in *Fusarium graminearum* Is Required for Female Fertility, Heterokaryon Formation, and Plant Infection. *Plant Physiology* 15(11), 1119–1127.
- [2] Braunwald MD, Marc A.Pfeffer MD, PhD (1991). Ventricular enlargement and remodeling following acute myocardial infarction: Mechanisms and management. *The American Journal of Cardiology*, Volume 68, Issue 14, 18 November 1991, Pages 1-6
- [3] Cleutjens JP. The role of matrix metalloproteinases in heart disease. *Cardiovasc Res* 1996;32:816-21. 8. B
- [4] Brown RD, Ambler SK, Mitchell MD, Long CS. The cardiac fibroblast: therapeutic target in myocardial remodeling and failure. *Annu Rev Pharmacol Toxicol* 2005;45:657-87.
- [5] Baudino TA, Carver W, Giles W, Borg TK. Cardiac fibroblasts: friend or foe? *Am J Physiol Heart Circ Physiol* 2006;291: H1015-26.
- [6] Camelliti P, Borg TK, Kohl P. Structural and functional characterization of cardiac fibroblasts. *Cardiovasc Res* 2005;65:40-51.
- [7] Cardiac Fibroblasts Bowers SL, Banerjee I, Baudino TA. The extracellular matrix: at the center of it all. *J Mol Cell Cardiol* 2010;48:474-82.
- [8] Tyagi SC. Proteinases and myocardial extracellular matrix turnover. *Mol Cell Biochem* 1997;168:1-12.
- [9] Sun Y, Weber KT. Infarct scar: a dynamic tissue. *Cardiovasc Res* 2000;46:250-6. Camelliti P, Borg TK, Kohl P. Structural and functional characterization of cardiac fibroblasts. *Cardiovasc Res* 2005;65:40-51.
- [10] Jugdutt BI. Remodeling of the myocardium and potential targets in the collagen degradation
- [11] Camelliti P, Borg TK, Kohl P. Structural and functional characterization of cardiac fibroblasts. *Cardiovasc Res* 2005;65:40-51.
- [12] Anderson KR, Sutton MG, Lie JT. Histopathological types of cardiac fibrosis in myocardial disease. *J Pathol* 1979;128:79-85.
- [13] Weber KT, Pick R, Jalil JE, Janicki JS, Carroll EP. Patterns of myocardial fibrosis. *J Mol Cell Cardiol* 1989;21(Suppl. 5):121-31.
- [14] van den Borne SW, Diez J, Blankesteyn WM, Verjans J, Hofstra L, Narula J. Myocardial remodeling after infarction: the role of myofibroblasts. *Nat Rev Cardiol* 2010;7:30-7.

- [15] Hou Z, Xue C, Peng Y, Katan T, Kistler HC, Xu JR. A mitogen activated protein kinase gene (MGV1) in *Fusarium gramine arum* is required for female fertility, heterokaryon formation, and plant infection. *Mol Plant Microbe Interact* 2002;15:1119-27.
- [16] Dobaczewski M, Bujak M, Zymek P, Ren G, Entman ML, Frangogiannis NG. Extracellular matrix remodeling in canine and mouse myocardial infarcts. *Cell Tissue Res* 2006;324:475-88.
- [17] Villarreal F, Omens J, Dillmann W, Risteli J, Nguyen J, Covell J. Early degradation and serum appearance of type I collagen fragments after myocardial infarction. *J Mol Cell Cardiol* 2004;36:597-601.
- [18] Clancy RM, Zheng P, O'Mahony M, Izmirly P, Zavadil J, Gardner L, et al. Role of hypoxia and cAMP in the transdifferentiation of human fetal cardiac fibroblasts: implications for progression to scarring in autoimmune-associated congenital heart block. *Arthritis Rheum* 2007;56:4120-31.
- [19] Willems IE, Havenith MG, De Mey JG, Daemen MJ. The alphasmooth muscle actin-positive cells in healing human myocardial scars. *Am J Pathol* 1994;145:868-75.
- [20] Torp-Pedersen C, Hansen FS, Pedersen A. Relation of left ventricular free wall rupture in acute myocardial infarction to forced immobilization. *Am J Cardiol* 1988;61:910-2.
- [21] Dan Kai, Molamma P Prabhakaran, Guorui Jin, Seeram Ramakrishna, Guided orientation of cardiomyocytes on electrospun aligned nanofibers for cardiac tissue engineering, Wiley Online Library
- [22] Y. Orlova, N. Magome, L. Liu, Y. Chen, K. Agladze, Electrospun nanofibers as a tool for architecture control in engineered cardiac tissue, 2011.
- [23] Marija Vulkicevic, PhD, Bobak Mosadegh, PhD, James k. Min, MD, Stephen H., Little, MD, Cardiac 3D Printing and its Future Directions 2017
- [24] D.G. Simpson, L. Terracio, M. Terracio, R.L. Price, D.C. Turner, T.K. Borg, Modulation of cardiac myocyte phenotype in vitro by the composition and orientation of the extracellular matrix, *J. Cell. Physiol.* 161 (1) (1994) 89–105
- [25] N. Bursac, K.K. Parker, S. Irvanian, L. Tung, Cardiomyocyte cultures with controlled macroscopic anisotropy: a model for functional electrophysiological studies of cardiac muscle, *Circ. Res.* 91 (12) (2002) e45–e54.
- [26] A. Marthur, Z. Ma, P. Loskill, S. Jeeawoody, K.E. Healy, *In vitro* cardiac tissue models: Current status and future prospects

- [27] Jugdutt BI. Remodeling of the myocardium and potential targets in the collagen degradation and synthesis pathways. *Curr Drug Targets Cardiovasc Haematol Disord* 2003;3:1-30. A. Eder, I. Vollert, A. Hansen, T. Eschenhagen, Human engineered heart tissue as a model system for drug testing, 2016
- [28] Clancy RM, Zheng P, O'Mahony M, Izmirly P, Zavadil J, Gardner L, et al. Role of hypoxia and cAMP in the transdifferentiation of human fetal cardiac fibroblasts: implications for progression to scarring in autoimmune-associated congenital heart block. *Arthritis Rheum* 2007;56:4120-31.
- [29] Camelliti P, Borg TK, Kohl P. Structural and functional characterization of cardiac fibroblasts. *Cardiovasc Res* 2005;65:40-51.
- [30] Zhen Ma, Sangmo Koo, Micaela A., Finnegan, Peter Loskill, Nathaniel Heusch, Natalie C. Marks, Bruce R. Conklin, Costas P. Grigoropoulos, Kevin E. Healy, Three-dimensional filamentous human diseased cardiac tissue model, 2014
- [31] Y. Orlova, N. Magome, L. Liu, Y. Chen, K. Agladze, Electrospun nanofibers as a tool for architecture control in engineered cardiac tissue, 2011.
- [32] I. C. Parrag, P. W. Zandstra, K. A. Woodhouse, Fiber alignment and coculture with fibroblasts improves the differentiated phenotype of murine embryonic stem cell-derived cardiomyocytes for cardiac tissue engineering, 2011.
- [33] A. Hussain, G. Collins, D. Yip, C. H. Cho, Functional 3-D cardiac co.culture model using bioactive chitosan nanofiber scaffolds, 2012.
- [34] M. Tallawi, E. Rosellini, N. Barbani, M. G. Cascone, R. Rai, G. Saint-Pierre, A. R. Boccaccini, Strategies for the chemical and biological functionalization of scaffolds for cardiac tissue engineering: a review, 2015.
- [35] Y. M. Shin, H. Park, H. Shin, Enhancement of cardiac myoblast responses onto electrospun PLCL fibrous matrices coated with polydopamine for gelatin immobilization, 2011.
- [36] D. A. Brown, R. E. Beygui, W. R. MacLellan, H. Laks, J. C. Y. Dunn, B. M. Wu, Modulation of gene expression in neonatal rat cardiomyocytes by surface modification of polyactide-*co*-glycolide substrates, 2004.
- [37] M. Boffito, F. Di Meglio, P. Mozetic, S. M. Giannitelli, I. Carmagnola, C. Castaldo, D. Nurzynska, A. M. Sacco, R. Miraglia, S. Montagnani, N. Vitale, M. Brancaccio, G. Terone, F. Basoli, A. Rainer, M. Trombetta, G. Ciardelli, V. Chiono, Surface functionalization of polyurethane scaffolds mimicking the myocardial microenvironment to support cardiac primitive cells, 2018.

- [38] A. Hussain, G. Collins, D. Yip. C. H. Cho, Functional 3-D cardiac co-culture model using bioactive chitosan nanofiber scaffolds, 2012.
- [39] Y. Orlova, N. Magome, L. Liu, Y. Chen, K. Agladze, Electrospun nanofibers as a tool for architecture control in engineered cardiac tissue, 2011.
- [40] E. Tarbit, I. Singh, J. N. Peart, R. B: Rose'Meyer, Biomarkers for the identification of cardiac fibroblast and myofibroblast cells, 2018.
- [41] Shimazaki M, Nakamura K, Kii I, Kashima T, Amizuka N, Li M, Saito M, Fukuda K, Nishiyama T, Kitajima S, Saga Y, Fukayama M, Sata M, Kudo A (2008) Periostin is essential for cardiac healing after acute myocardial infarction. *J Exp Med* 205(2):295–303
- [42] H. Zhao, X. Li, S. Zhao, Y. Zeng, L. Zhao, H. Ding, W. Sun, Y. Du, Microengineered *in vitro* model of cardiac fibrosis through modulating myofibroblast mechanotransduction, 2014.
- [43] C. k. Nagaraju, E. L. Robinson, M. Abdesselem, S. Trenson, E. Dries, G. Gilbert, S. Janssens, J. Van Cleemput, F. Rega, B. Meyns, H. L. Roderick, R. B. Driensen, K. R. Sipido, Myofibroblast phenotype and reversibility of fibrosis in patients with end-stage heart failure, 2019.
- [44] Z. Deng, Y.He, X. Yang, H. Shi, A. Shi, L. Lu, L. He, MicroRNA-29: A crucial player in fibrotic disease, 2017.
- [45] *In vitro* models of humancardiac fibrotic tissue on ‘bioartificial’ scaffolds, Biomedical Science and Engineering 2019; volume 3(s3):122 Alice Zoso,1-3 Irene Carmagnola,1-4 Gerardina Ruocco,1,2 Mattia Spedicati,1,2 Valeria Chiono1-4

Ringraziamenti

Per questo lavoro di tesi vorrei ringraziare la professoressa Valeria Chiono per la possibilità datami di lavorare ad un progetto così entusiasmante.

Ringrazio la dottoressa Irene Carmagnola per avermi seguito durante tutto il percorso. Un ringraziamento particolare va ai borsisti Gerardina Ruocco e Mattia Spedicati che hanno fatto un lavorone nel seguirmi, nell'essere presenti in tutte le situazioni e per aver dato un grosso contributo nel lavoro di revisione della tesi, facendosi in quattro tra tutti gli impegni. Ringrazio tutto il personale del dipartimento di Ingegneria Meccanica e Aerospaziale (DIMEAS) e il laboratorio La.Di.Spe. In particolare, ringrazio Giulia, Letizia, Michela e Viola per la loro disponibilità e simpatia.

Un ringraziamento speciale va a mamma Rosanna e papà Adriano che sono stati sempre presenti senza mai essere invadenti, cosa molto difficile per un genitore, sono sempre riusciti ad essere le guide perfette che ognuno dovrebbe avere, senza farmi mai mancare niente. Ringrazio mio fratello Marco che è stato sempre uno dei miei migliori amici sempre presente sin da quando eravamo piccoli. Ringrazio Federica, che mi ha ascoltato lamentarmi tutti i giorni consigliandomi in tutte le situazioni. Grazie a Giovanni e Simone coinquilini storici con cui ho condiviso tutte le disgrazie e le piccole gioie.

Ringrazio gli amici di sempre, quelli che ogni volta che tornavo erano sempre presenti, Christian, il cuore del gruppo, che mi ha fatto capire che è possibile fare tutto quando si ha la passione, Mirko, che mi ha dimostrato che non si è mai troppo grandi per perdere a cod, e Lorenzo, che mi ha spiegato "ca alla Svizzera nu ete comu quai".

Ringrazio tutte le persone che ho incontrato durante questo traguardo, quelle che sono rimaste fino alla fine e quelle che hanno preso strade diverse. Ringrazio tutti i balenotteri, Alessio, Andrea, Daniele, Davide, Elia, Giovanni, Graziano, Luca e Valentino per avere animato le mie serate torinesi e per aver reso la mia vita universitaria così emozionante. Grazie a Cristina e Federica le ragazze del vecchio terzo piano, che ci hanno fatto da spalla. Per ultimo vorrei ringraziare mia nonna che è stata la mia roccia fino a qualche anno fa, ma che se ancor presente non potrà gioire per il mio traguardo, ma che sono sicuro che a suo modo le avrebbe fatto piacere sapere dove sono arrivato. Ma soprattutto la ringrazio perché mi ha dimostrato, con il suo esempio, che non bisogna mai tirarsi indietro nel sacrificarsi per aiutare chi ci è vicino, perché alla fine non è importante il traguardo che raggiungi o la fama che ottieni, ma sono importanti le persone che ti circondano e che sapranno starti accanto quando la vita farà sentire il suo peso.